Biogeosciences, 11, 3757–3779, 2014
www.biogeosciences.net/11/3757/2014/
doi:10.5194/bg-11-3757-2014

Biogeosciences Open Access

On the effects of circulation, sediment resuspension and biological incorporation by diatoms in an ocean model of aluminium*

M. M. P. van Hulten[1], A. Sterl[1], R. Middag[2,3,4], H. J. W. de Baar[4,5], M. Gehlen[6], J.-C. Dutay[6], and A. Tagliabue[7]

[1]Royal Netherlands Meteorological Institute (KNMI), Utrechtseweg 297, 3731 GA De Bilt, the Netherlands
[2]University of Otago, 364 Leith Walk, Dunedin, 9016, New Zealand
[3]University of California Santa Cruz (UCSC), 1156 High Street, Santa Cruz, CA 95064, USA
[4]Royal Netherlands Institute for Sea Research (NIOZ), Landsdiep 4, 1797 SZ 't Horntje, Texel, the Netherlands
[5]University of Groningen (RUG), Postbus 72, 9700 AB Groningen, the Netherlands
[6]Laboratoire des Sciences du Climat et de l'Environnement (LSCE), LSCE-Orme, point courrier 129, CEA-Orme des Merisiers, 91191 Gif-sur-Yvette Cedex, France
[7]University of Liverpool, 4 Brownlow Street, Liverpool L69 3GP, UK

*Postprints may be found at http://arxiv.org/abs/1405.5752

Correspondence to: M. M. P. van Hulten (marco@hulten.org)

Received: 12 July 2013 – Published in Biogeosciences Discuss.: 2 September 2013
Revised: 23 May 2014 – Accepted: 5 June 2014 – Published: 18 July 2014

Abstract. The distribution of dissolved aluminium in the West Atlantic Ocean shows a mirror image with that of dissolved silicic acid, hinting at intricate interactions between the ocean cycling of Al and Si. The marine biogeochemistry of Al is of interest because of its potential impact on diatom opal remineralisation, hence Si availability. Furthermore, the dissolved Al concentration at the surface ocean has been used as a tracer for dust input, dust being the most important source of the bio-essential trace element iron to the ocean. Previously, the dissolved concentration of Al was simulated reasonably well with only a dust source, and scavenging by adsorption on settling biogenic debris as the only removal process. Here we explore the impacts of (i) a sediment source of Al in the Northern Hemisphere (especially north of $\sim 40°$ N), (ii) the imposed velocity field, and (iii) biological incorporation of Al on the modelled Al distribution in the ocean. The sediment source clearly improves the model results, and using a different velocity field shows the importance of advection on the simulated Al distribution. Biological incorporation appears to be a potentially important removal process. However, conclusive independent data to constrain the Al / Si incorporation ratio by growing diatoms are missing. Therefore, this study does not provide a definitive answer to the question of the relative importance of Al removal by incorporation compared to removal by adsorptive scavenging.

1 Introduction

One of the first interesting findings of the now ongoing GEOTRACES programme is the remarkable mirror image between the distributions of dissolved aluminium (Al_{diss}) and dissolved silicic acid (Si_{diss}) in the West Atlantic Ocean (Fig. 1), which suggests a close interaction between the two tracers. As Si_{diss} is a major nutrient for diatom growth, it is important to understand this interaction. An initial effort towards understanding this distribution of Al_{diss} has been accomplished by using an ocean circulation–biogeochemistry model (Van Hulten et al., 2013). The model only had one source, aeolian dust input at the surface, and one sink, scavenging by adsorption on settling biogenic debris. This provided a reasonable agreement with the measurements of [Al_{diss}]. However, very high [Al_{diss}] near the seafloor in the 40–50° N region was not well reproduced, which suggests that an additional source term of Al supply from the underlying sediments in this region is required. Furthermore, there is ample evidence and debate in the literature on the biological

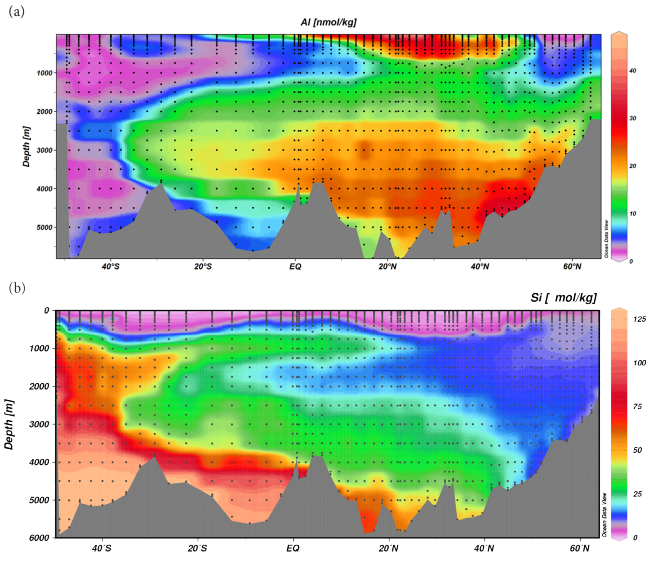

Figure 1. Observations of **(a)** $[Al_{diss}]\,(nmol\,kg^{-1})$ and **(b)** $[Si_{diss}]\,(\mu mol\,kg^{-1})$ at the West Atlantic GEOTRACES transect (Middag et al., 2014). Dots are the locations of the measurements.

incorporation of Al into the opaline ($SiO_2 \cdot nH_2O$) frustules of growing diatoms in ocean surface waters, and/or merely post-depositional Al enrichment of fossil opal deposits in the sediments. The importance of these processes needs to be evaluated. Finally, in the previous simulation the model distributions of Si_{diss} deviated significantly from the observed distribution (Fig. 1b), most likely due to imperfections in the circulation of the model.

The cycling and distribution of aluminium in the ocean has received attention for several reasons, among which are the interactions between the cycles of aluminium (Al) and silicon (Si). Dissolved Al is scavenged by adsorption onto biogenic debris that settles as aggregates into the deep ocean, henceforth called Al_{ads} (e.g. Stoffyn and Mackenzie, 1982; Orians and Bruland, 1986; Hydes et al., 1988). In addition, dissolved Al becomes incorporated into biological opal ($SiO_2 \cdot nH_2O$), primarily in the frustules of diatoms (e.g. Stoffyn, 1979; Hydes et al., 1988; van Beusekom and Weber, 1992; Koning et al., 2007). The Al incorporated in opal of living diatoms is hereafter called Al_{diat}. The relatively heavy opal (twice the density of seawater) serves as ballast for settling aggregates; it removes the adsorbed as well as the incorporated Al efficiently. This is consistent with the reduced levels of dissolved Al, in regions of high diatom production (e.g. Orians and Bruland, 1986). Conversely, the rate of dissolution of settling opal debris (hereafter called biogenic silica, Si_{biog}) appears to be controlled by the Al / Si element ratio of this opal. The higher the Al / Si ratio of opal, the lower the rate of Si_{biog} dissolution (e.g. Lewin, 1961; van Bennekom et al., 1991; Dixit et al., 2001; Gehlen et al., 2002).

Another major reason of interest in Al is the use of Al as a tracer of aeolian dust supply into the surface ocean, which is an important source of iron and other trace nutrients. Indeed, it is currently assumed that the major source of Al to the open ocean is dust deposition (e.g. Kramer et al., 2004; de Jong et al., 2007). A fraction of the Al in dust (1–15 %) dissolves within the upper mixed layer (e.g. Orians and Bruland, 1986; Maring and Duce, 1987; Baker et al., 2006; Han et al., 2012). Below the mixed layer the dissolution of Al from dust is deemed negligible. The remaining 85–99 % fraction of Al remains in the particulate, lithogenic phase and sinks to the bottom of the ocean where it is assumed to be buried in the sediment.

The second source of Al is hypothesised to be sediment resuspension and subsequent release, e.g. by desorption, from previously sedimented Al (Moran and Moore, 1991; Middag et al., 2012, 2014). Such a source can be contrasted with diffusion from sediments, which typically occurs only for redox-active elements like iron and manganese. Indeed, a high concentration of dissolved aluminium (Al_{diss}) has been measured near the deep sediment in the West Atlantic Ocean at 45–50° N (Fig. 1a), while Al is not redox-active. One prerequisite is sufficient turbulence near the sediment. This is satisfied at several locations in the West Atlantic Ocean (Fig. 2). Especially north of $\sim$35° N and south of $\sim$40° S, significant resuspension of sediment occurs (Biscaye and Eittreim, 1977; Gross et al., 1988). Another obvious prerequisite is an adequate supply of sedimenting Al towards the seafloor. Even though lithogenic particulate Al from dust deposition is such a supply, Al in that form is relatively refractory, meaning that it is not easily released (Brown and Bruland, 2009). Hence, sedimenting Al associated with Si_{biog} is a more obvious candidate for the sediment source of Al_{diss}. The scavenger and incorporator of Al, the Si_{biog}, is mostly present alongside active diatom production: north of 44° N and south of 40° S (Nelson et al., 1995; Tréguer and De La Rocha, 2013). Therefore, in these regions this prerequisite is satisfied.

There appears to be variability in the sediment source of Al. Generally, $[Al_{diss}]$ is significantly higher near the sediment compared to concentrations 500 m above the sediment. However, the elevation of $[Al_{diss}]$ near the sediments of the Southern Ocean is very small compared to its elevation in the Atlantic Ocean (Moran et al., 1992; Middag et al., 2011b). This strongly suggests that in the Southern Hemisphere the desorption of Al from Al_{ads} from resuspended sediments is very small compared to the desorption in the Atlantic Ocean. Upon settling on the seafloor, the desorption of adsorbed aluminium is hypothesised to be controlled by the concentration of dissolved silicon in ambient seawater. At a higher dissolved Si concentration, the desorption of Al is reduced (Mackin and Aller, 1986). Especially in the Antarctic Bottom Water (AABW), the $[Si_{diss}]$ is very high, preventing desorption of Al. Biogenic silica may also play a role in preventing desorption of Al, since (adsorbed) Al is incorporated in biogenic silica (Koning et al., 2007). Understanding these

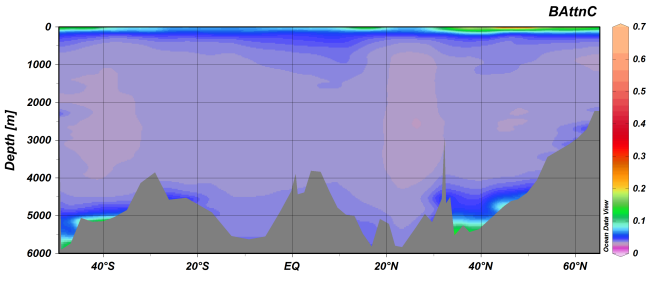

Figure 2. Beam attenuation coefficient, a measure of the amount of particles (e.g. Behrenfeld et al., 2006). Courtesy of Micha Rijkenberg.

interactions is important for understanding the cycling of Si and hence the primary production of diatoms.

Other sources do not appear to play a significant role in adding Al to the ocean. Even though rivers carry a large amount of Al, most of it is removed in estuaries and continental shelf sediments, and never enters the open ocean (Mackin, 1986; Orians and Bruland, 1986; Brown et al., 2010; Jones et al., 2012). Finally, hydrothermal vents are not a source of Al to the deep waters of the oceans either (Hydes et al., 1986; Lunel et al., 1990; Elderfield and Schultz, 1996; Middag et al., 2011a).

The primary removal mechanism of Al_{diss} from the surface ocean is the adsorptive scavenging and settling with Si_{biog} as the major carrier. Therefore this removal is large in areas with high diatom production (Stoffyn and Mackenzie, 1982; Orians and Bruland, 1986; Moran and Moore, 1988a, 1989, 1992). Besides being scavenged by surface adsorption, the Al_{diss} becomes incorporated as a trace substitute for Si during growth of living diatoms (e.g. Stoffyn, 1979; van Beusekom and Weber, 1992; Chou and Wollast, 1997; Gehlen et al., 2002; Koning et al., 2007; Middag et al., 2009). However, it is not always clear how significant the effect of incorporation is (Vrieling et al., 1999; Moran and Moore, 1988b; Ren et al., 2011). Following diatom mortality, the incorporated Al, then referred to as biogenic Al (Al_{biog}), is exported with the Si_{biog} debris. These processes are schematically presented in Fig. 3.

Incorporated Al is likely to inhibit the dissolution of Si_{biog} (Lewin, 1961; van Bennekom et al., 1991; van Beusekom and Weber, 1992; Dixit et al., 2001). This means that at a high Al_{diat} / Si_{diat} ratio in living diatoms and consequent same ratio of Al_{biog} / Si_{biog} in biogenic debris, less Si_{biog} will be remineralised. Moreover, more silica will be buried and hence lost from the system. Consequently, less Si_{diss} will be returned to the surface through upwelling, resulting in decreased diatom production. This highlights the major link between Al and Si.

Recent years have seen the development of models of the marine biogeochemical cycle of aluminium. For the Al removal, Gehlen et al. (2003) and Van Hulten et al. (2013) implemented a scavenging model, while Han et al. (2008) included both scavenging and biological incorporation of Al into the frustules of diatoms.

Gehlen et al. (2003) had the objective of testing the sensitivity of modelled Al fields to dust input and thus of evaluating the possibility of constraining dust deposition via dissolved Al near the ocean's surface. For this purpose they embedded an Al cycle in the HAMOCC2 biogeochemical model (Maier-Reimer, 1993). The Al model consists of a reversible first-order relation of adsorption of Al_{diss} onto Si_{biog}. In chemical equilibrium the Al_{ads} concentration is proportional to the product of the concentrations of Al_{diss} and particulate Si_{biog}. The resulting modelled concentration of Al_{diss} was of the same order of magnitude as the then published observations. The model of Van Hulten et al. (2013) used the same chemical equilibrium relation between adsorbed and dissolved Al. Instead of testing the effect of different dust fields, they tested the sensitivity to the solubility of Al from dust in the ocean surface and in the water column. This constrained the percentage and depth of dissolution of Al from the dust. The coefficient partitioning Al_{ads} and Al_{diss} was constrained as well with the respective sensitivity simulation. A sensitivity simulation with a margin sediment source showed that margin sediments are probably not an important source of Al. The main goal of Han et al. (2008) was to better constrain the dust deposition field. For this purpose they used the Biogeochemical Elemental Cycling (BEC) model improved by Moore and Braucher (2008) as a starting point. This was used in combination with the Dust Entrainment And Deposition (DEAD) model to explicitly constrain dust deposition. In addition to scavenging, Han et al. (2008) added a biological Al uptake module where the Al / Si uptake ratio is a function of the ambient dissolved Al and Si concentrations. However, they did not expand on the importance of biological incorporation relative to adsorptive scavenging.

These recently developed models are consistent with the first principles of Al cycling in the ocean, showing that the dissolution of Al from dust and the reversible scavenging by Si_{biog} can reproduce the main features of the observed Al_{diss} concentration. However, the deep ocean has not been simulated very well, and significant numbers of accurate deep ocean measurements of [Al_{diss}] have only become available recently (e.g. Middag et al., 2009). Furthermore, some studies raise doubts about the scavenging nature of Al removal from the ocean (e.g. Koning et al., 2007).

Recent high-accuracy observations from the West Atlantic Ocean GEOTRACES transect show a mirror image between [Al_{diss}] and [Si_{diss}] (Fig. 1). The key observation from this transect data is that Si_{diss} is a nutrient type (enriched in old water) and Al a scavenged type element (depleted in older water). Furthermore, the mirror image suggests that (i) there is a very modest sediment source of Al where [Si_{diss}] is relatively high, i.e. where the AABW prevails flowing from Antarctica up to 45° N, and (ii) the Denmark Strait Overflow Water (DSOW) brings bottom waters with low [Si_{diss}] from the Denmark Strait (∼ 66° N) to at least 45° N. The latter, in

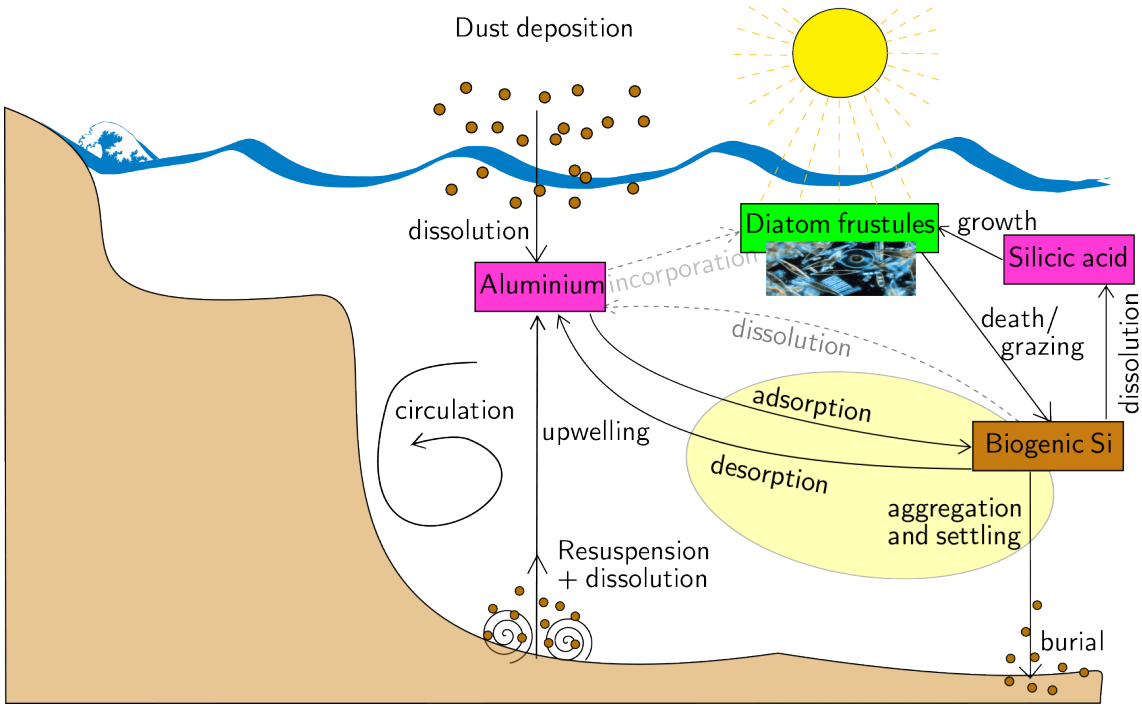

Figure 3. Aluminium cycling in the ocean. Dissolved Al enters the ocean through the release of Al_{diss} from deposited dust and resuspended sediments, while rivers, hydrothermal vents and reducing sediments are negligible sources of Al_{diss}. Al is mostly removed by reversible scavenging (presented in the yellow ellipse). The dashed arrow from aluminium to diatom frustules signifies incorporation of Al into diatom frustules. Silicic acid (Si_{diss}) is presented as well, since it is an essential part of understanding Al cycling. However, not all sources of Si_{diss} are presented in this figure.

combination with ample supply of adsorbed Al from opal debris of diatom blooms in overlying surface waters, appears to result in major desorption of Al from resuspended particles in the bottom waters (Middag et al., 2014).

The other process of interest is that of biological incorporation of Al by diatoms. The goal in this research is to assess whether this is a significant process. A simulation with incorporation is expected to yield a decrease of $[Al_{diss}]$ compared to the simulation without incorporation. The decrease may even result in an unrealistically low $[Al_{diss}]$ since scavenging parameters were tuned in the reference simulation to fit the open ocean main thermocline distribution of Al_{diss} and most of the West Atlantic GEOTRACES transect at full depth.

In this study the model of Van Hulten et al. (2013) is extended with three major changes. The different simulations address the role of circulation, the importance of a sediment source and the significance of biological incorporation of Al by diatoms. Details on this model and of the observational data set are given in Sect. 2. Next, the results of the reference simulation and the three sensitivity simulations, relative to the reference simulation and to the simulation in Van Hulten et al. (2013), are presented in Sect. 3. More discussion about the model assumptions and the simulation results is to be found in Sect. 4. Finally, Sect. 5 ends with the major conclusions.

2 Methods

2.1 Model description

2.1.1 Model framework

In order to simulate the three-dimensional distribution of dissolved Al, the biogeochemical model PISCES is used (Aumont and Bopp, 2006; Ethé et al., 2006). This model has been employed for many other studies concerning trace metals, as well as large-scale ocean biogeochemistry (e.g. Aumont and Bopp, 2006; Gehlen et al., 2007; Arsouze et al., 2009; Dutay et al., 2009; Tagliabue et al., 2010). In the simulations described here, PISCES has been driven by climatological velocity fields obtained from the general circulation model called Nucleus for European Modelling of the Ocean (NEMO) (Madec, 2008) of which the dynamical component is called Océan PArallélisé (OPA) (Madec et al., 1998).

The model PISCES simulates the cycle of carbon, the major nutrients (nitrate, phosphate, ammonium, silicic acid) and the trace nutrient iron, along with two phytoplankton types (nanophytoplankton and diatoms), two zooplankton grazers (micro- and mesozooplankton), two classes of particulate organic carbon (small and large) of differential settling velocities, as well as calcite and biogenic silica. The PISCES model distinguishes three silicon pools: (i) the silicon content of

living diatoms (Si_{diat}); (ii) the silicon content of dead, settling diatoms (Si_{biog}) and (iii) dissolved silicic acid (Si_{diss}). In the model, Si_{diss} and other nutrients are supplied to the ocean by means of atmospheric dust deposition and rivers, while iron enters the ocean as well through sediment remobilisation (Aumont and Bopp, 2006). The standard version of PISCES accounts for 24 tracers. For a more detailed description of PISCES see the auxiliary material of Aumont and Bopp (2006).

In this study PISCES is run off-line forced by a climatological year of monthly physical fields including turbulent diffusion. All model fields are defined on the ORCA2 grid, an irregular grid covering the whole world ocean with a nominal resolution of $2^\circ \times 2^\circ$, with the meridional (south–north) resolution increased near the equator. It has two "north poles" in Canada and Russia to eliminate the coordinate singularity in the Arctic Ocean. Its vertical resolution is 10 m in the upper 100 m, increasing downwards to 500 m, such that there are 30 layers in total and the ocean has a maximum depth of 5000 m.

2.1.2 Aluminium model

The Al model is based on the preceding model of Van Hulten et al. (2013) which computes the concentration of dissolved aluminium (Al_{diss}) and adsorbed Al (Al_{ads}). In this study two additional tracers are introduced to PISCES: the Al incorporated in the opaline frustules of living diatoms (Al_{diat}) and its biogenic debris (Al_{biog}). All tracer names are listed in Table 1. For completeness, the Si tracers in PISCES are given as well. The concentrations of the tracers are indicated by square brackets [ ], and are given in units of $\mathrm{mol\,dm^{-3}}$ (shortly M or molar).

There are two different sources of Al in the model. One source is via the dissolution of dust particles in the upper ocean layer. The dust deposition field was taken from the output of the atmospheric dust model INCA (Hauglustaine et al., 2004; Textor et al., 2006). The other source, which has now been added to the previous model, is sediment resuspension and subsequent dissolution. When Al_{ads} reaches the ocean floor, it is assumed to be buried, except for the resuspension and subsequent dissolution of Al in some simulations. The model is schematically represented in Fig. 3, where the extensions to Van Hulten et al. (2013) are resuspension/desorption (bottom-left) and biological incorporation (top-right). Sediment and porewater reactions are not explicitly modelled. Resuspension and subsequent desorption take place in the water column.

The model parameters are listed in Table 2.

The aluminium fraction in dust (f_{Al}) is based on the mass percentages of Al known to be present in the Earth's crust. This is about 8.1 % aluminium by mass on average (Wedepohl, 1995). Most of this Al consists of oxides that do not dissolve easily. The fraction of Al from dust (α_{Al}) that dissolves is not well constrained but is probably in the range of 1–15 % (Orians and Bruland, 1986; Jickells et al., 2005). Here $\alpha_{Al} = 5\,\%$ is chosen, since this is has been successfully used in previous modelling work (Han et al., 2008; Van Hulten et al., 2013). The dissolution occurs only in the upper model layer (0–10 m depth range), and is described by

$$\left.\frac{\partial[\mathrm{Al_{diss}}]}{\partial t}\right|_{\mathrm{deposition}} = \frac{\alpha_{\mathrm{Al}} f_{\mathrm{Al}}}{m_{\mathrm{Al}} \Delta z_1} \Phi_{\mathrm{dust}}, \quad (1)$$

where m_{Al} is the atomic mass of Al, $\Delta z_1 = 10$ m is the thickness of the surface model layer and Φ_{dust} is the dust flux into the ocean. The Al that does not dissolve from dust is assumed to play no role in the biogeochemical cycle of Al on our timescales of interest, and can be thought of as being buried in marine sediments.

Another source of Al is sediment resuspension (bottom-left in Fig. 3). In reality, this is induced by near-sediment turbulence, creating a 200–1000 m thick nepheloid layer above the sediment containing significant amounts of suspended sediment particles (e.g. Lampitt, 1985; Hwang et al., 2010). However, here it is assumed that recently settled Al_{ads} is resuspended and subsequently partly dissolved in the bottom model layer. Since the resuspension depends on settling of Al_{ads}, the relevant model equation will be introduced at the end of this section, after the settling equation.

Dissolved Al is assumed to adsorb onto biogenic silica particles, while other particles do not have an effect on the removal of Al_{diss} (discussed in Van Hulten et al. (2013) and Sect. 4). Hence, aside from external inputs (and optionally the incorporation within the silica), the Al_{diss} concentration is governed by adsorption and desorption (yellow ellipse in Fig. 3). The Al_{diss} and Al_{ads} concentrations are governed by the following reversible first-order adsorption equation (Van

Table 1. Aluminium and silicon tracers in the model.

Tracer	Description
Al_{diss}	dissolved Al: ions and colloids with $\emptyset < 0.2\,\mu m$
Al_{ads}	Al adsorbed onto biogenic silica
Al_{diat}	Al incorporated in frustules of living diatoms
Al_{biog}	Al incorporated in frustules of dead diatoms
Si_{diss}	dissolved Si, or silicic acid
Si_{diat}	Si incorporated in frustules of living diatoms
Si_{biog}	Si incorporated in frustules of dead diatoms

Table 2. Parameters for the reference simulation RefDyn2 (identical to those of RefDyn1).

Parameter	Symbol	Value
Mass fraction of Al in dust	f_{Al}	8.1 %
Surface dissolution fraction	α_{Al}	5 %
Partition coefficient	k_d	$112 \times 10^3\ \mathrm{M^{-1}}$
First-order rate constant	κ	$10^4\ \mathrm{yr^{-1}}$
Settling speed of Al_{ads} and Al_{biog}	w_s	30–200 $\mathrm{m\,d^{-1}}$

Hulten et al., 2013):

$$\frac{\partial[\mathrm{Al_{ads}}]}{\partial t}\Big|_{\mathrm{ad/desorption}} = \kappa(A^{\mathrm{eq}}_{\mathrm{ads}} - [\mathrm{Al_{ads}}]), \tag{2}$$

where

$$A^{\mathrm{eq}}_{\mathrm{ads}} = k_{\mathrm{d}} \cdot [\mathrm{Al_{diss}}] \cdot [\mathrm{Si_{biog}}], \tag{3}$$

in which $A^{\mathrm{eq}}_{\mathrm{ads}}$ is the chemical equilibrium concentration of $\mathrm{Al_{ads}}$. The parameter k_{d} ($\mathrm{dm^3\,mol^{-1}}$) is the partition coefficient and κ ($\mathrm{s^{-1}}$) is the first-order rate constant for equilibration of $[\mathrm{Al_{ads}}]$ to $A^{\mathrm{eq}}_{\mathrm{ads}}$. Finally, $\mathrm{Si_{biog}}$ is the biogenic silica concentration, as with all concentrations, in $\mathrm{mol\,dm^{-3}}$. Since total Al is conserved when only internal processes are concerned, the time derivative of $[\mathrm{Al_{diss}}]$ equals the negative of that of $[\mathrm{Al_{ads}}]$.

As an extension to the original model, aluminium is incorporated into the frustules of diatoms during production. The diatom incorporation of Al is modelled by multiplying the rate of production of diatom opal ($\mathrm{Si_{diat}}$) with the dissolved Al / Si concentration ratio in ambient seawater, with some refinements as explained below. For the biological Si cycle, production and mortality (including grazing by micro- and mesozooplankton) of diatoms, and dissolution of debris $\mathrm{Si_{biog}}$, are represented by prod, mort and diss, respectively, in Eq. (4). All rate variables are proportional to the ratio of Al and Si in the relevant source pool. Accordingly, the biological model equations for Al are as follows:

$$\frac{\partial[\mathrm{Al_{diat}}]}{\partial t}\Big|_{\mathrm{bio}} = R_{\mathrm{Al/Si}} \cdot \mathrm{prod} - \frac{[\mathrm{Al_{diat}}]}{[\mathrm{Si_{diat}}]} \cdot \mathrm{mort} \tag{4a}$$

$$\frac{\partial[\mathrm{Al_{biog}}]}{\partial t}\Big|_{\mathrm{bio}} = \frac{[\mathrm{Al_{diat}}]}{[\mathrm{Si_{diat}}]} \cdot \mathrm{mort} - \frac{[\mathrm{Al_{biog}}]}{[\mathrm{Si_{biog}}]} \cdot \mathrm{diss} \tag{4b}$$

$$\frac{\partial[\mathrm{Al_{diss}}]}{\partial t}\Big|_{\mathrm{bio}} = \frac{[\mathrm{Al_{biog}}]}{[\mathrm{Si_{biog}}]} \cdot \mathrm{diss} - R_{\mathrm{Al/Si}} \cdot \mathrm{prod}. \tag{4c}$$

No further refinement is made in any process, except, optionally, for incorporation during production. This is accomplished by the incorporation ratio $R_{\mathrm{Al/Si}}$, which is defined as

$$R_{\mathrm{Al/Si}} = \min\left(c_{\mathrm{in}} \cdot \frac{[\mathrm{Al_{diss}}]}{[\mathrm{Si_{diss}}]},\ r_{\mathrm{max}}\right), \tag{5}$$

where $[\mathrm{Al_{diss}}]/[\mathrm{Si_{diss}}]$ is the ratio of dissolved Al and Si, and c_{in} ($0 \le c_{\mathrm{in}} \lesssim 1$) is an optional weight factor for the Al:Si incorporation ratio and $r_{\mathrm{max}} \ge 0$ is an optional prescribed maximum value for the $\mathrm{Al_{diat}}/\mathrm{Si_{diat}}$ ratio within the opal of living diatoms. These two optional parameters are not used in the model simulations presented in this work (i.e. we use $c_{\mathrm{in}} = 1$ and $r_{\mathrm{max}} = \infty$), but will be discussed in Sect. 4.3.1 on biological incorporation. The biological extension to the model is schematically presented in Fig. 3 as the dotted line from "Aluminium" to "Diatom frustules".

Both $\mathrm{Al_{biog}}$ and $\mathrm{Al_{ads}}$ settle through the water column, because the concurrent biogenic silica is denser than seawater. Adsorbed and incorporated Al (their concentrations both denoted as A_{part}) settle along with biogenic silica with a velocity w_{s}, varying from 30 $\mathrm{m\,d^{-1}}$ in the upper 100 m to 200 $\mathrm{m\,d^{-1}}$ at 4 km below the mixed layer, according to

$$\frac{\partial A_{\mathrm{part}}}{\partial t}\Big|_{\mathrm{settling}} = -w_{\mathrm{s}} \frac{\partial A_{\mathrm{part}}}{\partial z}\,. \tag{6}$$

While settling through the water column, $\mathrm{Al_{biog}}$ and $\mathrm{Al_{ads}}$ may in the process remineralise (Eqs. 4b and 2, respectively), so adsorption and incorporation do not mean that all Al is removed immediately from the model domain. Part of the Al dissolves and may upwell, and may become incorporated or scavenged once again at a later time.

Burial of $\mathrm{Al_{ads}}$ and $\mathrm{Al_{biog}}$ proceeds in the bottom model layer immediately above the sediment according to

$$\frac{\partial A_{\mathrm{part}}}{\partial t} = -\frac{w_{\mathrm{s}} \cdot A_{\mathrm{part}}}{\Delta z_{\mathrm{bottom}}}\,, \tag{7}$$

where $\Delta z_{\mathrm{bottom}} \le 500$ m is the thickness of the bottom layer. It is of the same order of magnitude as the real resuspension, or nepheloid, layer. In two of the simulations, part of the sedimented $\mathrm{Al_{ads}}$ is resuspended and dissolved in the bottom water layer according to

$$\frac{\partial[\mathrm{Al_{diss}}]}{\partial t}\Big|_{\mathrm{resusp}} = \beta \cdot \frac{w_{\mathrm{s}} \cdot [\mathrm{Al_{ads}}]}{\Delta z_{\mathrm{bottom}}}, \tag{8}$$

where β is a constant ($0 < \beta \le 1$), or some scalar function to be defined later (Eq. 9), representing the fraction of resuspended and subsequently dissolved Al. Note that in the model only adsorbed Al is redissolved, while biogenic Al is not (see Sect. 4.2.2 for rationale). This process is different from the sediment source in Van Hulten et al. (2013). In that study sediment input was modelled analogously to the diffusive iron source, while in this study the redissolution depends on freshly sedimented $\mathrm{Al_{ads}}$. The underlying rationale and the derivation of Eq. (8) are given in Appendix A. Moreover, silicic acid near the sediment apparently inhibits the dissolution of $\mathrm{Al_{ads}}$. This is probably because $\mathrm{Al_{diss}}$ and $\mathrm{Si_{diss}}$ are stoichiometrically saturated (Mackin and Aller, 1986). Observations suggest a significant Al sediment source below Denmark Strait Overflow Water (DSOW) where $\mathrm{Si_{diss}}$ concentrations are below 30 µM (1 µM = 10^{-6} $\mathrm{mol\,dm^{-3}}$), while they suggest only a very weak source from the sediment below AABW, which has much higher $[\mathrm{Si_{diss}}]$, exceeding 50 µM (Middag et al., 2014). In one of the simulations, the bottom water $[\mathrm{Si_{diss}}]$ will be used as an inhibitor of the redissolution of Al from resuspended sediment.

The source code of the model is included as an electronic supplement. This code can be used with NEMO-PISCES (in this study version 3.1 was used), to be found at http://www.nemo-ocean.eu/ (libre software licensed under CeCILL).

2.1.3 Simulations

The reference simulation (RefDyn2) is based on the "reference experiment" from Van Hulten et al. (2013) (RefDyn1),

but there is one notable improvement. A different set of dynamical fields (advection, turbulent diffusion and mixing) is now used. The velocity fields used by Van Hulten et al. (2013) (Dynamics 1) had an Atlantic Meridional Overturning Circulation (MOC) that is too shallow and too weak, while the northward flux of AABW is too strong, compared to estimates based on measurements. The fields used in this study, henceforth referred to as Dynamics 2, are a climatology from a NEMO-OPA simulation forced by the DFS3 air–sea fluxes (Large and Yeager, 2004; Uppala et al., 2005; Brodeau et al., 2010). Dynamics 2 has a more realistic Atlantic overturning, compared to Dynamics 1. Firstly, the depth of North Atlantic Deep Water is about 2 km in Van Hulten et al. (2013) while it is closer to the more reasonable 3 km in the dynamics used here. Secondly, the maximum of the Atlantic Overturning Stream Function (OSF) in the AABW dropped from about 6–7 Sv in Dynamics 1 to about 2–3 Sv in Dynamics 2, much more comparable to estimates based on observations (Talley et al., 2003; Rayner et al., 2011). This results in a significantly better simulation of the Si_{diss} distribution (see discussion in Sect. 4.1.1). The Si_{diss} concentration in AABW is much closer to the observational concentration, compared with the dynamical fields used by Van Hulten et al. (2013) (basic statistics for the West Atlantic Ocean are presented in Sect. 3.2). This will especially be important for one of the sediment resuspension simulations described below, since that simulation depends on $[Si_{diss}]$ in bottom water.

The reference simulation (RefDyn2) is initialised from the steady-state concentrations of the reference experiment in Van Hulten et al. (2013) (RefDyn1), and is then run for another 1750 model years to steady state with Dynamics 2. The resulting total Al budget (both dissolved and adsorbed) in the world ocean in the reference simulation is around 6 Tmol (1 Tmol = 10^{12} mol). After 1000 yr of simulation the Al budget (total Al_{diss} + Al_{ads} integrated over the ocean volume) does not change much (less than 1 % before reaching steady state). Therefore, from year 1000 our two sets of sensitivity simulations with sediment resuspension and biological incorporation are forked and run for another 500 yr, alongside the reference simulation, to quasi-steady state. An overview of the simulations with the key parameters is given in Table 3, and the two sets of sensitivity simulations are defined and explained below.

The dust dissolution and scavenging parameters as used by Van Hulten et al. (2013) resulted in a good simulation of $[Al_{diss}]$ in the upper ocean. Therefore, the same parameters were used for the new reference simulation (RefDyn2, Table 2). This is also the case for most sensitivity simulations, except for IncorpLowScav where the partition coefficient k_d is decreased. A sediment source is included in simulations SedProp and SedMackin, and biological incorporation of Al is present in the simulations Incorp and IncorpLowScav (Table 3).

In the first of our two sediment resuspension simulations, 60 % of sedimented Al_{ads} is redissolved just above the sediment ($\beta = 0.60$, see Eq. 8). This means that redissolution is proportional to sedimentation, hence this simulation is named SedProp. However, the West Atlantic Ocean GEOTRACES observations show a large elevation of $[Al_{diss}]$ due to resuspension only in the Northern Hemisphere and only very little in the Southern Hemisphere (Fig. 1a). It appears that the process of release of Al from resuspended sediments is inhibited in the Southern Hemisphere. As shown by Mackin and Aller (1986), the inhibition may be caused by high $[Si_{diss}]$, which is very high in the AABW in the Southern Hemisphere and flows as far north as $\sim 40°$ N, albeit somewhat diluted by vertical mixing with overlying NADW that has lower Si_{diss} concentrations. Therefore the result of Mackin and Aller (1986) is used to arrive at the following dissolution fraction:

$$\beta = \beta_0 ([Si_{diss}]_{bottom}/\mu M)^{-0.828}, \quad (9)$$

where β_0 is a dimensionless constant (in this simulation set to 16.85) and the -0.828 is from Mackin and Aller (1986). For further discussion see the derivation in Appendix A and the discussion in Sect. 4.2. Henceforth this simulation is referred to as SedMackin.

Finally, one set of two simulations with biological incorporation of Al into diatom frustules has been performed. In these simulations Al_{diss} is scavenged in the same way as in the other simulations. No limitation to the incorporation of Al_{diss} has been applied. This means that for these simulations, $c_{in} = 1$ and $r_{max} = \infty$ (see Eq. 5), such that $R_{Al/Si} = [Al_{diss}]/[Si_{diss}]$; alternatives will be discussed in Sect. 3. The first of two incorporation simulations, Incorp, is with the normal scavenging parameters. The second one, IncorpLowScav, is different with respect to Incorp in that the partition

Table 3. Overview of the two reference simulations as defined in the text, and the two sets of sensitivity simulations as defined later in the text. If not specified otherwise, when the term reference simulation is used, we refer to RefDyn2. Here RefDyn1 refers to the old "reference experiment" of Van Hulten et al. (2013). Dynamics 1 refers to the climatology based on ERS satellite data; Dynamics 2 is based on DFS3. The Si_{diss}-dependence refers to the dependence on bottom water $[Si_{diss}]$ for dissolution of resuspended adsorbed Al. The normal partition coefficient is $k_d = 112 \times 10^3$ dm^3 mol^{-1}. This is equivalent to the $k_d = 4 \times 10^6$ dm^3 kg^{-1} in Van Hulten et al. (2013), where the biogenic Si concentration was denoted in kg dm^{-3} instead of mol dm^{-3}. For consistency in the concentration units, we changed the unit (and hence the value) of k_d.

Simulation	Dynamics	Sediment	Si_{diss}-dependent	Incorporation	k_d
RefDyn1	1	no	–	no	normal
RefDyn2	2	no	–	no	normal
SedProp	2	yes	no	no	normal
SedMackin	2	yes	yes	no	normal
Incorp	2	no	–	yes	normal
IncorpLowScav	2	no	–	yes	normal/4

coefficient is decreased from 112 to 28×10^3 dm^3 mol^{-1}, for reasons that will become clear in Sect. 3.

2.2 Observational data sets

Recent GEOTRACES observations of [Al_{diss}] in the Arctic Ocean (Middag et al., 2009), Northeast Atlantic Ocean (Middag, 2010, Chapter 5), West Atlantic Ocean (Middag et al., 2014), the Atlantic sector of the Southern Ocean (Middag et al., 2011b, 2012, 2013) and the region south of Australia (Remenyi, 2013) are used for a detailed comparison and optimisation of the model parameters. See the upper part of Table 4 for these data sets. These data sets comprise overall 4013 individual data values for dissolved Al. All values have been verified versus international reference samples and their consensus values of the SAFe and GEOTRACES programmes. See Van Hulten et al. (2013) for more details. In addition to the data sets used by Van Hulten et al. (2013), the GEOTRACES International Polar Year (GIPY) data by Remenyi (2013) (data and dissertation on request available from lead author) have been added to the data set, namely SAZ-Sense (GIPY2) and SR3 (GIPY6). Those data are located between Tasmania and Antarctica (438 data points). Furthermore, there are five additional stations (120 extra data points) in the Northwest Atlantic Ocean (64 PE 358). These additional cruises add up to 558 extra data points, compared to the number used by Van Hulten et al. (2013).

For a worldwide global ocean comparison one also has to rely on data that were collected in the era before the reference samples of SAFe and GEOTRACES were available. Inevitably, the criteria for selecting such previously published data sets are less strict; see Van Hulten et al. (2013) and Middag (2010, 216–218) for the criteria used for each of the selected data sets. The selected pre-GEOTRACES data sets are listed in the lower part of Table 4.

Table 4. Observational data used for comparison with model.

Cruise	Ocean	Source	#
ARK XXII/2	Arctic	Middag et al. (2009)	1080
ANT XXIV/3	Southern	Middag et al. (2011b)	919
SAZ-Sense	Southern	Remenyi (2013)	146
SR3	Southern	Remenyi (2013)	292
64 PE 267	Atlantic	Middag et al. (2014)	137
64 PE 319	Atlantic	Middag et al. (2014)	383
64 PE 321	Atlantic	Middag et al. (2014)	504
64 PE 358	Atlantic	Middag et al. (2014)	120
JC057	Atlantic	Middag et al. (2014)	432
Subtotal used primarily for detailed comparison			4013
IOC96	Atlantic	Vink and Measures (2001)	1048
M 60	Atlantic	Kremling (1985)	91
IRONAGES III	Atlantic	Kramer et al. (2004)	181
EUCFe	Pacific	Slemons et al. (2010)	195
MC-80	Pacific	Orians and Bruland (1986)	92
VERTEX-4	Pacific	Orians and Bruland (1986)	54
VERTEX-5	Pacific	Orians and Bruland (1986)	59
KH-98-3	Indian	Obata et al. (2007)	152
Subtotal of other observations for global comparison			1872
Grand total of all dissolved Al values			5885

2.3 Data–model comparison

For the, mostly qualitative, visual comparison between model and observations, horizontal and vertical cross sections of the model data are plotted. For the horizontal [Al_{diss}] sections four different depths are presented, where "surface" signifies the average over the upper 30 m, "500 m" is 400–600 m averaged, "2500 m" is 2300–2700 m averaged and "4500 m" is 4000–5000 m averaged. The respective observations (same depth ranges) are presented as coloured dots. The colour scale is not linear to better show the main features at both low and high concentrations of Al_{diss}.

The vertical [Al_{diss}] sections are of the GEOTRACES cruises in the West Atlantic Ocean (64 PE 267, 319, 321, 358; and JC057 from Table 4) and the Zero Meridian Southern Ocean (part of ANT XXIV/3). These sections are calculated from the three-dimensional model data by converting the ORCA2-gridded model data to a rectilinear mapping, and interpolating the rectilinear data onto the cruise track coordinates. One of these figures also shows the Atlantic Overturning Stream Function (OSF), defined as the zonally (through the Atlantic Ocean) and vertically (from the surface downward) integrated meridional current speed. This is used as a measure for the MOC.

The focus of this study is the West Atlantic Ocean for several reasons. Firstly, recently measurements have been carried out in that region, resulting in a large consistent (one method) data set. Secondly, there are too few high-quality observations in other regions of the ocean, making it very difficult to define a reasonable goodness of fit. Thirdly, the West Atlantic Ocean is of large importance to the MOC and hence the deep ocean cycling of nutrients. For these reasons all quantitative arguments in this study concern the West Atlantic GEOTRACES transect.

2.3.1 Statistics

To compare quantitatively the model results with the observations, we focus only on the 1576 data points of the West Atlantic Ocean GEOTRACES transect (Sect. 3). First the observations are linearly interpolated onto the model grid. Then several statistics are determined, namely the root mean square deviation (RMSD), the reliability index (RI) and the correlation coefficient r^2. These statistics are all based on Stow et al. (2009), but the first two are adjusted for the inhomogeneous sample distribution in depth.

The RMSD is determined by the following equation:

$$D_{\updownarrow} = \sqrt{\frac{\sum_{k=1}^{30} \Delta z_k \cdot \sum_{j=1}^{60} (m_{jk} - o_{jk})^2}{60 \cdot \sum_{k=1}^{30} \Delta z_k}}, \quad (10)$$

where o is the observed and m the modelled [Al_{diss}], weighting with model layer thickness Δz_k of layer $k \in \{1 \ldots 30\}$ for every station $j \in \{1 \ldots 60\}$. The $\updownarrow$ signifies the vertical weighting modification of the standard RMSD. This is done to compensate for the over-representation of data points near the ocean surface. Furthermore, for each sensitivity simulation we calculate the significance of the change in the RMSD compared with the corresponding reference simulation. This is determined by means of a Monte Carlo simulation on the reference simulation for which a subsample of 400 has been randomly selected from the original set of 1800 data–model points. They are the pairs of observations and model data, both on the model grid. This is done 50 000 times and from this the 2σ confidence interval is calculated (the mean $\pm$ two times the standard deviation). Suppose that we wish to simulate q, and assume q is in steady state. For each model Y resulting in $q_Y(\mathbf{x})$, the average RMSD of the Monte Carlo simulation of $q_Y(\mathbf{x})$ must be outside the 2σ confidence range of the RMSD distribution of $q_X(\mathbf{x})$ to say that Y is a significant improvement or worsening compared to X.

The reliability index adjusted by weighting with the model layer thickness is defined as

$$\mathrm{RI}_{\updownarrow} = \exp \sqrt{\frac{\sum_{k=1}^{30} \Delta z_k \sum_{j=1}^{60} (\log \frac{o_{jk}}{m_{jk}})^2}{60 \cdot \sum_{k=1}^{30} \Delta z_k}}. \quad (11)$$

Finally, the correlation coefficient is defined as

$$r = \frac{\sum_{i=1}^{1800} (o_i - \overline{o})(m_i - \overline{m})}{\sqrt{\sum_{i=1}^{1800} (o_i - \overline{o})^2 \sum_{i=1}^{1800} (m_i - \overline{m})^2}}, \quad (12)$$

where 1800 is the total number of measurements of the West Atlantic GEOTRACES transect and the bars denote averages.

3 Results

In this section the results of the simulations are presented. The relevant tracers of the raw model output can be found at http://data.zkonet.nl/index.php?page=Project_view&id=2916&tab=Datasets.

3.1 Reference simulation and observations

Figure 4 shows the modelled yearly average steady-state Al_{diss} concentration of RefDyn2 at four depths versus observations as coloured dots. In Fig. 5 the GEOTRACES transects in the West Atlantic Ocean and the Zero Meridian Southern Ocean are presented. At the surface of the Atlantic Ocean, the highest modelled and measured [Al_{diss}] is located from near the equator northwards to about 35° N. In the polar oceans and in the South Pacific Ocean, [Al_{diss}] is very low. At the West Atlantic transect, the MOC is clearly reflected by the dissolved Al concentration. The decrease of [Al_{diss}] from north to south in the North Atlantic Deep Water (NADW) is due to net adsorptive scavenging onto settling biogenic silica.

The similarity between the model (RefDyn2) and the observations decreases in the deeper North Atlantic Ocean, where according to the observations [Al_{diss}] increases with depth (for depths below 800 m), while in the model the dissolved Al concentration decreases with depth. Besides this general pattern of increasing [Al_{diss}] with depth in the observations, a very high concentration of Al_{diss} is present between 45 and 50° N near the sediment, which enhances the dissimilarity between the reference simulation and the observations.

3.2 Improved dynamics

In this reference simulation (RefDyn2) Dynamics 2 was used. This forcing has its maximum southward transport at a reasonably realistic depth of almost 3 km (contour in Fig. 5), while Van Hulten et al. (2013) used a forcing with the strongest southward transport closer to 2 km (Dynamics 1). The more reasonable OSF depth results in an improved simulation of [Al_{diss}] in the West Atlantic Ocean (Fig. 5). The RMSD of [Al_{diss}] of the reference simulation from Van Hulten et al. (2013) (RefDyn1) versus observations is 8.3 nM, while the RMSD of this new simulation (RefDyn2) versus observations is 8.7 nM. The difference between these RMSD values is insignificant (Table 5).

The first two rows in Table 5 present the goodness of fit statistics for [Si_{diss}]. Inspecting the RMSD, RefDyn2 of this study appears a significant improvement over RefDyn1 of Van Hulten et al. (2013). The improved Si_{diss} distribution gives credibility to the [Si_{diss}]-dependent sediment resuspension simulation (also: Sect. 4.1.1). Since [Si_{diss}] is improved, it is likely that the Si cycle as a whole is improved, but an assessment of the Si cycle is beyond the scope of this paper.

3.3 Sediment resuspension

Figure 6 shows the [Al_{diss}] resulting from the simulation in which sediment resuspension is proportional to $w_s Al_{ads}/\Delta z_{bottom}$ just above the sediment (SedProp).

In the Northern Hemisphere, the deep [Al_{diss}] is simulated much better in this simulation than in RefDyn2 (Fig. 5), but in the Southern Hemisphere [Al_{diss}] is simulated much worse. The dissolved Al concentration is too high near the bottom, and elevated [Al_{diss}] levels are found throughout the whole water column. Nonetheless, the addition of resuspension in this way does significantly improve the simulation ($D_{\updownarrow}$ = 5.2 nM, compared to 8.7 nM for the reference

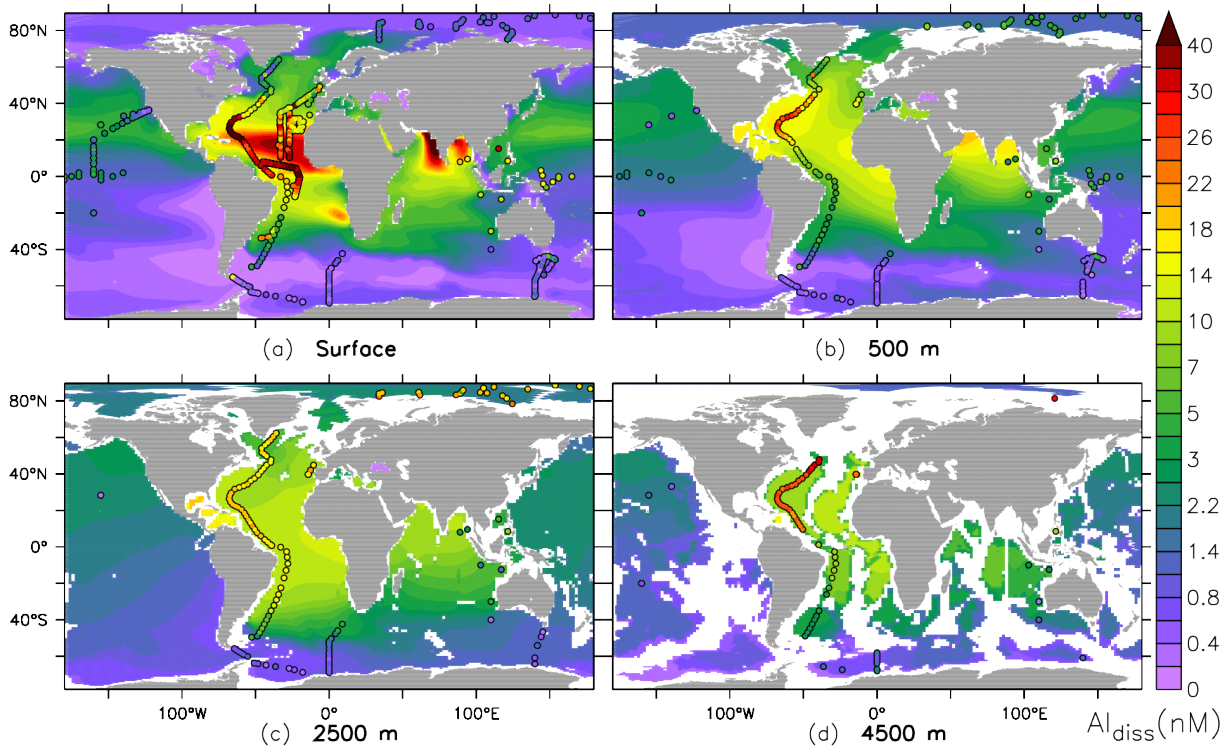

Figure 4. Average of the final model year (1750) of the dissolved aluminium concentration (nM) from the reference simulation (RefDyn2) at four depths. The respective observations (same depth ranges) are presented as coloured dots.

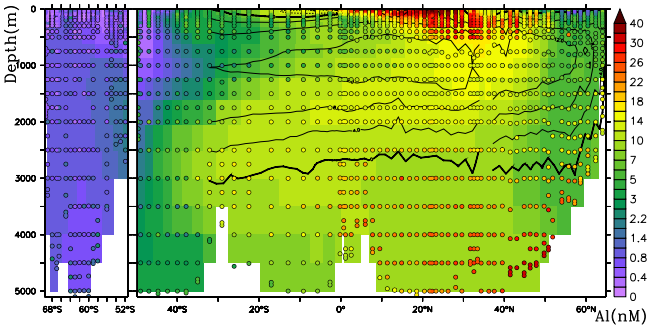

Figure 5. Dissolved aluminium concentration (nM) from RefDyn2 (simulated year 1750) along the Zero Meridian and West Atlantic GEOTRACES transect. Observations are presented as coloured dots. The contour is the Atlantic overturning stream function (OSF), only defined north of Cape Agulhas and away from 36° N where cross-land mixing through the unresolved Strait of Gibraltar does not allow for a well-defined OSF.

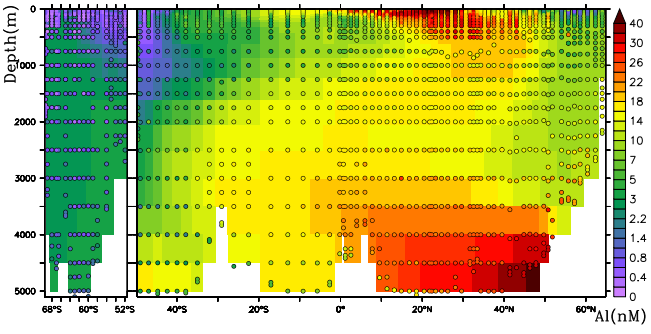

Figure 6. Simulated [Al$_{diss}$] (nM) from the [Si$_{diss}$]-independent sediment resuspension simulation (500 yr after forking) along the Zero Meridian and West Atlantic GEOTRACES transect (SedProp). Observations are represented by the coloured dots.

simulation). However, in the southern Atlantic Ocean and along the Zero Meridian in the Southern Ocean, sediment input should be much closer to zero.

Figure 7a shows [Al$_{diss}$] from simulation SedMackin, where sedimentary Al addition depends on bottom water [Si$_{diss}$] according to Mackin and Aller (1986) (β as defined by Eq. 9). As expected, also in SedMackin the sediment resuspension source of Al results in a higher [Al$_{diss}$] near 40–50° N in the deep North Atlantic Ocean (Fig. 7b) compared to RefDyn2. However, several characteristics of the observations are better reproduced by SedMackin than SedProp. Firstly, in the Southern Hemisphere, the [Al$_{diss}$] is only slightly elevated near the sediment compared to the overlying water (Fig. 7a). The observations extend to practically the bottom of the ocean, almost 6000 m at some latitudes of the West Atlantic GEOTRACES transect, while the model depth is only 5000 m. This makes a good comparison of deep

Table 5. Statistics of [Si_{diss}] (first two rows) and [Al_{diss}] (other rows) of the simulations in the West Atlantic GEOTRACES transect. Here D is the unweighted RMSD, $D_{\updownarrow}$ the vertically homogenised RMSD (accompanied with its significance compared with $D_{\updownarrow}$ from the first row of each subtable, and the 2σ range), r is the correlation coefficient, RI the reliability index and $RI_{\updownarrow}$ is the vertically homogenised reliability index. The significance is with respect to the first simulation in the corresponding subtable.

Simulation	D	$D_{\updownarrow}$	*Significance*$_{\updownarrow}$	2σ *range*$_{\updownarrow}$	r	RI	$RI_{\updownarrow}$
[Si_{diss}]:							
RefDyn1 (Van Hulten et al., 2013)	23.8 µM	39.7 µM	–	[34.8, 44.4]	0.70	4.05	2.57
RefDyn2 (this study)	12.7 µM	18.0 µM	improvement	[15.8, 20.2]	0.77	4.02	2.07
[Al_{diss}]:							
RefDyn1	7.4 nM	8.3 nM	–	[7.5, 9.2]	0.71	2.00	1.91
RefDyn2	8.9 nM	8.7 nM	insignificant	[7.9, 9.6]	0.71	2.10	1.98
RefDyn2	8.9 nM	8.7 nM	–	[7.9, 9.6]	0.71	2.10	1.98
SedProp	7.0 nM	5.2 nM	improvement	[4.6, 5.8]	0.75	1.97	1.68
SedMackin	7.1 nM	5.9 nM	improvement	[5.2, 6.4]	0.74	2.02	1.69
Incorp	13.1 nM	11.1 nM	worsening	[10.2, 12.0]	0.62	3.33	2.80
IncorpLowScav	11.7 nM	9.4 nM	insignificant	[8.6, 10.1]	0.61	2.35	2.08

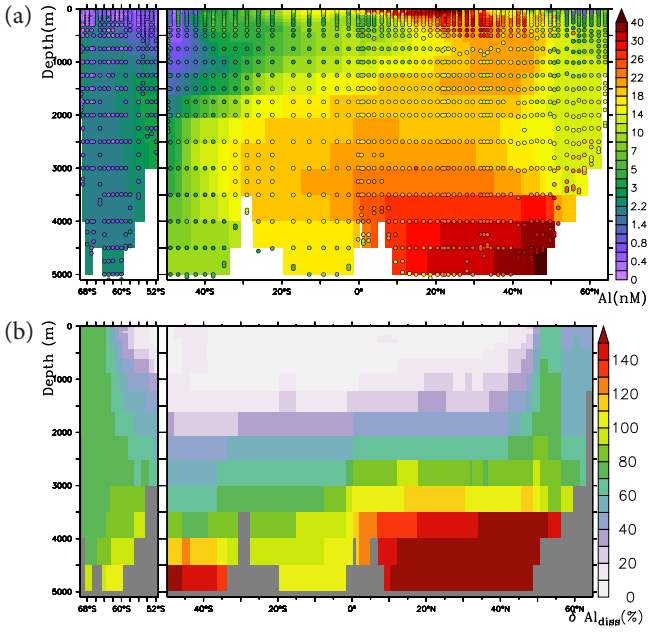

Figure 7. Results from the [Si_{diss}]-dependent sediment resuspension simulation following Mackin and Aller (1986) of year 500 after forking; sections along the Zero Meridian and West Atlantic GEOTRACES transects. **(a)** Modelled [Al_{diss}] (nM) with observations plotted as coloured dots. **(b)** Relative difference of [Al_{diss}] between SedMackin and RefDyn2 (%).

ocean [Al_{diss}] between model and observations difficult, but the slightly elevated [Al_{diss}] in the near-sediment observations is consistent with the slight elevation that is mainly confined to the bottom model layer. Secondly, the region from 0–45° N at a depth below 2 km has a higher [Al_{diss}] compared to the reference simulation (Fig. 7b) and better represents the observations.

Based on the low [Si_{diss}] alone, a high near-sediment [Al_{diss}] is expected north of 50° N as well. Indeed, this is the case in the observations, but it is not found in the model. This could be related to the relatively low resolution of the model which does not resolve well the dynamical (advection and deep convection) and, related, biogeochemical processes in this region. As expected, the resuspended Al_{diss} mixes into the (lower) NADW, but most of it is scavenged again before reaching the equator (Fig. 7b). The overall resulting [Al_{diss}] is more consistent with the observations compared to the original simulation (RefDyn2) without any sediment resuspension. For RefDyn2, $D_{\updownarrow} = (8.8 \pm 0.8)$ nM, while for the sediment resuspension simulations, $D_{\updownarrow} = 5.2$ nM and $D_{\updownarrow} = 5.9$ nM, which are statistically significant improvements (see Table 5).

Figure 8 shows the [Al_{diss}] at four depths for SedMackin, with observations as coloured dots. Figure 9 shows the difference of [Al_{diss}] between this simulation and the reference simulation. In several semi-enclosed basins, like the Gulf of Mexico and the Arctic Ocean, and the Atlantic Ocean, [Al_{diss}] is higher compared to the reference simulation, especially near the sediment. The Gulf of Mexico, the Mediterranean Sea, Baffin Bay and the Arctic Ocean may contribute to [Al_{diss}] in the Atlantic Ocean. However, the increase of near-sediment [Al_{diss}] in the West Atlantic Ocean at 45–50° N is much more likely caused by in situ resuspension and subsequent dissolution (Fig. 7b).

Several statistics show that SedMackin is an improvement over RefDyn2 (Table 5). This, together with the presented concentration plots, shows that the sediment redissolution process is an improvement of the model. This lends support to the hypothesis of a sediment source of Al in the form of

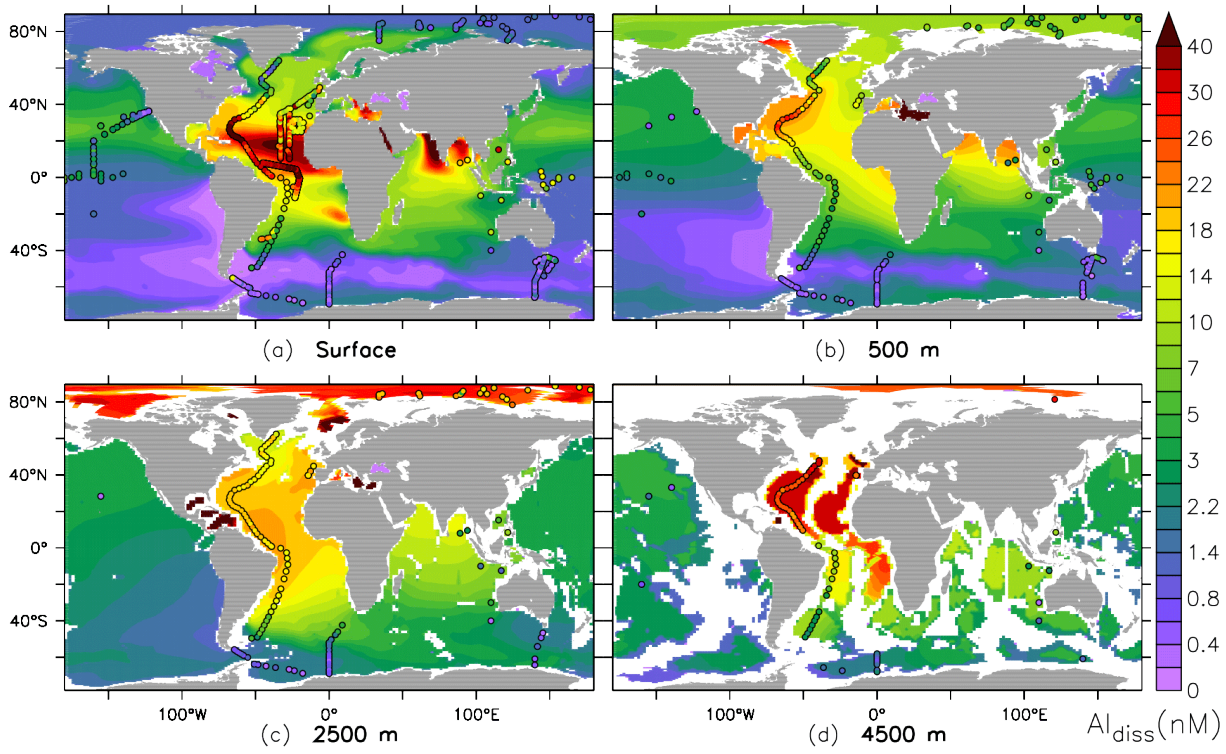

Figure 8. [Al$_{diss}$] (nM) of the [Si$_{diss}$]-dependent simulation with sediment resuspension (SedMackin) at four depths (500 yr after forking).

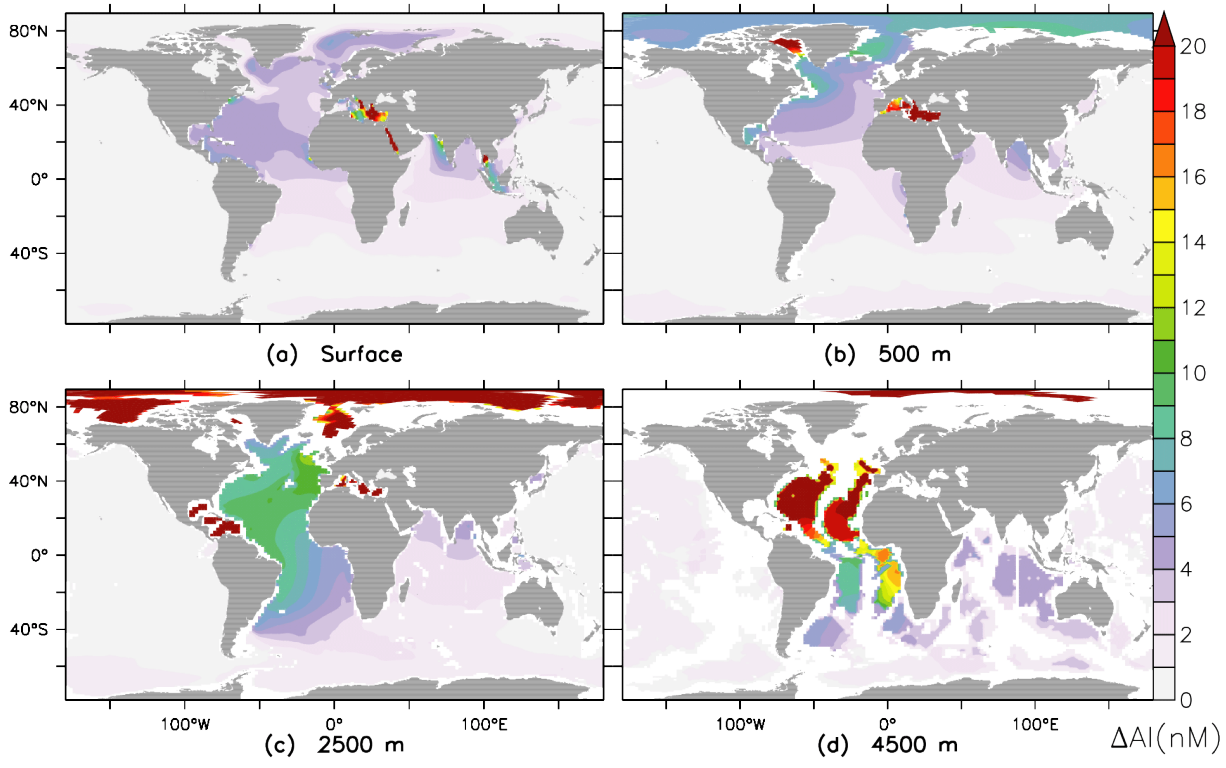

Figure 9. Difference of [Al$_{diss}$] (nM) between the simulation with [Si$_{diss}$]-dependent sediment resuspension (SedMackin) and the reference simulation at four depths (500 yr after forking).

resuspension and subsequent dissolution in the real ocean. In most of the deep ocean (Fig. 8c and d) the model overestimates the observations. However, the statistics do not show an improvement of SedMackin over SedProp. Apparently the choice of $\beta_0 = 16.85$ is too high, which only showed up after a sufficiently long spin-up of the model. It would require several more trial and error model runs to arrive by iteration to the optimal value of β_0, but this is beyond the scope of this paper.

3.4 Biological incorporation

The relative difference between the simulated $[Al_{diss}]$ with and without biological incorporation is presented in Fig. 10 at four depths. In the main thermocline, north of 60° S, $[Al_{diss}]$ is significantly lower with incorporation than without (Fig. 10a, b). While the reference simulation RefDyn2 simulates the observed $[Al_{diss}]$ well in the upper part of the ocean, in the simulation Incorp a large amount of Al is removed by incorporation in addition to adsorptive scavenging from the upper part of the ocean.

The significantly lower $[Al_{diss}]$ in the main thermocline in Incorp, compared with RefDyn2, makes the modelled concentrations much lower than the observed concentrations. This suggests that incorporation may not occur (to such an extent), which is consistent with the findings of Vrieling et al. (1999). This result does not prove that biological incorporation of Al by diatoms does not occur. It only means that this way of incorporating Al into the frustules in this model with its current configuration yields an unrealistically low value of $[Al_{diss}]$. There are several possibilities to compensate this effect so that future simulations may still be compatible with the incorporation hypothesis. Notably, the amount of Al incorporated into the frustules may need to be significantly reduced, or the scavenging parameters need to be adjusted, or dust dissolution must be increased. The result of a simulation with a decreased partition coefficient is presented next. Further discussion of the three options can be found in Sect. 4.3.

Figure 11 presents the relative concentration difference between IncorpLowScav and RefDyn2. The decrease in the Atlantic Ocean surface waters is slightly smaller than in the case with incorporation and a high k_d (compare with Fig. 10). However, in the Southern Ocean the $[Al_{diss}]$ has increased relatively by a considerable amount, yielding concentrations much higher than the observed concentrations.

The RMSD between IncorpLowScav and the observations (at the West Atlantic GEOTRACES transect) is 9.4 nM. Even though this is a significant improvement compared to Incorp, it is only the case when absolute residuals are considered (RMSD). When the correlation coefficient is considered, IncorpLowScav ($r = 0.61$) appears not to be an improvement over Incorp ($r = 0.62$). In fact, the correlation coefficient for IncorpLowScav is the lowest of all simulations. Indeed, IncorpLowScav shows poor model performance in the Southern Hemisphere (Fig. 10). Compared to the simulation without incorporation (RefDyn2), the run with incorporation with fourfold lower partition coefficient (IncorpLowScav) performs poorly. This degradation in model performance is insignificant when the RMSD is considered (which considers absolute residuals). Dimensionless goodness of fits like the reliability index RI or the correlation coefficient r do not show any significant improvement or worsening of IncorpLowScav either, compared with RefDyn2 (significance values not presented). Finally, decreasing the first-order rate constant κ has a very similar effect as decreasing k_d (results not presented).

From these considerations it may be concluded, within the limitations of the model, that if incorporation is an important process at all, it is unlikely to occur proportional to the ambient $[Al_{diss}]/[Si_{diss}]$ ratio in surface seawater but rather in a much smaller ratio (i.e. $c_{in} \ll 1$ in Eq. (5) as further discussed in Sect. 4.3.1).

4 Discussion

4.1 General biogeochemistry

4.1.1 Underlying model

Clearly, besides the dust solubility, the scavenging parameters and resuspension parameterisation, the Al model depends on the dynamics (Sect. 3.2) and the underlying biogeochemical model as well. Both the dynamics and the biogeochemical model have a strong impact on $[Si_{diss}]$. Figure 12 presents modelled $[Si_{diss}]$ for both dynamical fields, with measured $[Si_{diss}]$ as coloured dots.

Clearly Fig. 12a, corresponding with Dynamics 1, shows a strongly overestimated $[Si_{diss}]$ in the deep ocean, while this overestimation is significantly reduced in Fig. 12b (Dynamics 2). The reason for this is that in Dynamics 2 the northward flux of AABW is smaller and does not go as far northwards as Dynamics 1. Hence, less Si_{diss}, which is rich in AABW, reaches the northern parts of the deep Atlantic Ocean. In other words, the more realistic deep overturning cell in Dynamics 2 results in a more realistic simulation of $[Si_{diss}]$ in the deep Atlantic Ocean (Table 5). Even though we have improved the Si_{diss} distribution by using a different dynamical forcing, the absolute value of the deep $[Si_{diss}]$ does not match very well the observations. At most places in the deep West Atlantic Ocean, $[Si_{diss}]$ still overestimates the observations (Fig. 12b). For the sediment resuspension simulation SedMackin, this has been taken into account by modifying the proportionality factor β_0 (Eq. 9). Still, β_0 was estimated somewhat too high as noted above.

The Si_{biog} concentration is important as well for the Al model, namely for scavenging. However, there is no consistent observational data set of $[Si_{biog}]$. Available data (e.g. Lam, 2011) generally report particulate silica as the sum of biogenic silica (diatom frustules) and silica mineral phases

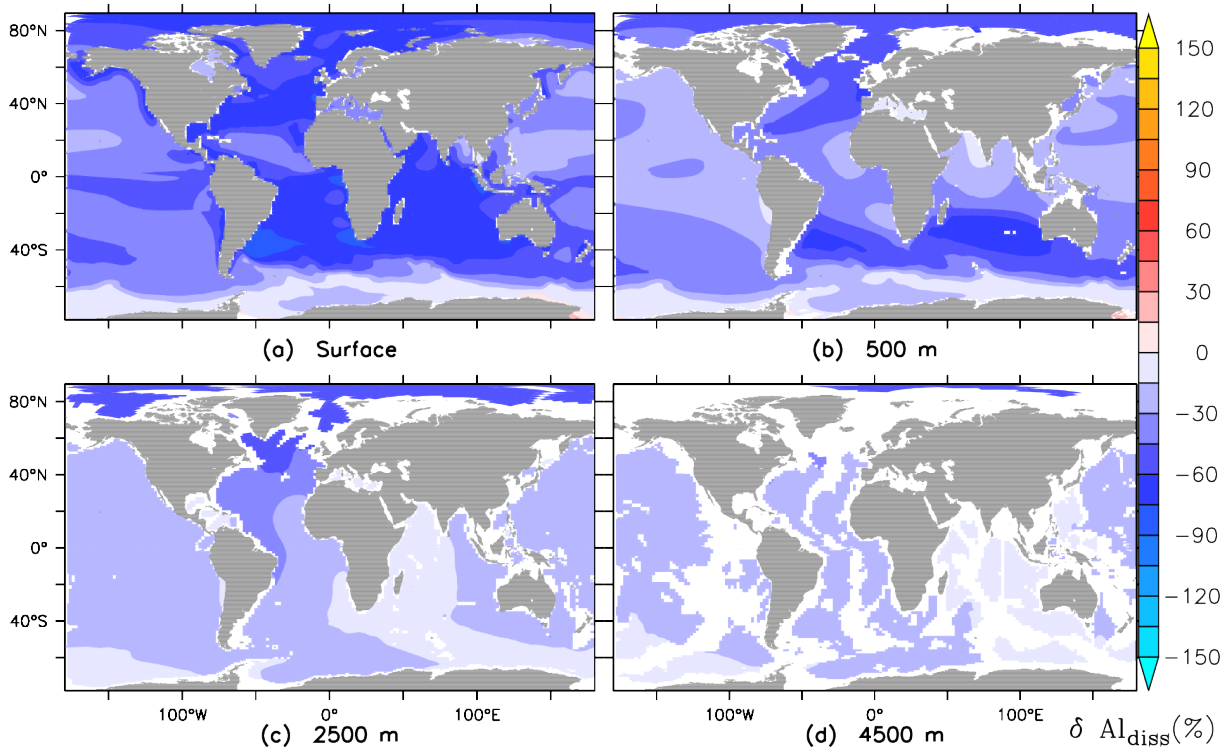

Figure 10. Relative difference of $[Al_{diss}]$ (%) between the simulation with biological incorporation (Incorp) and the reference simulation (RefDyn2) at four ocean depths (average over year 500).

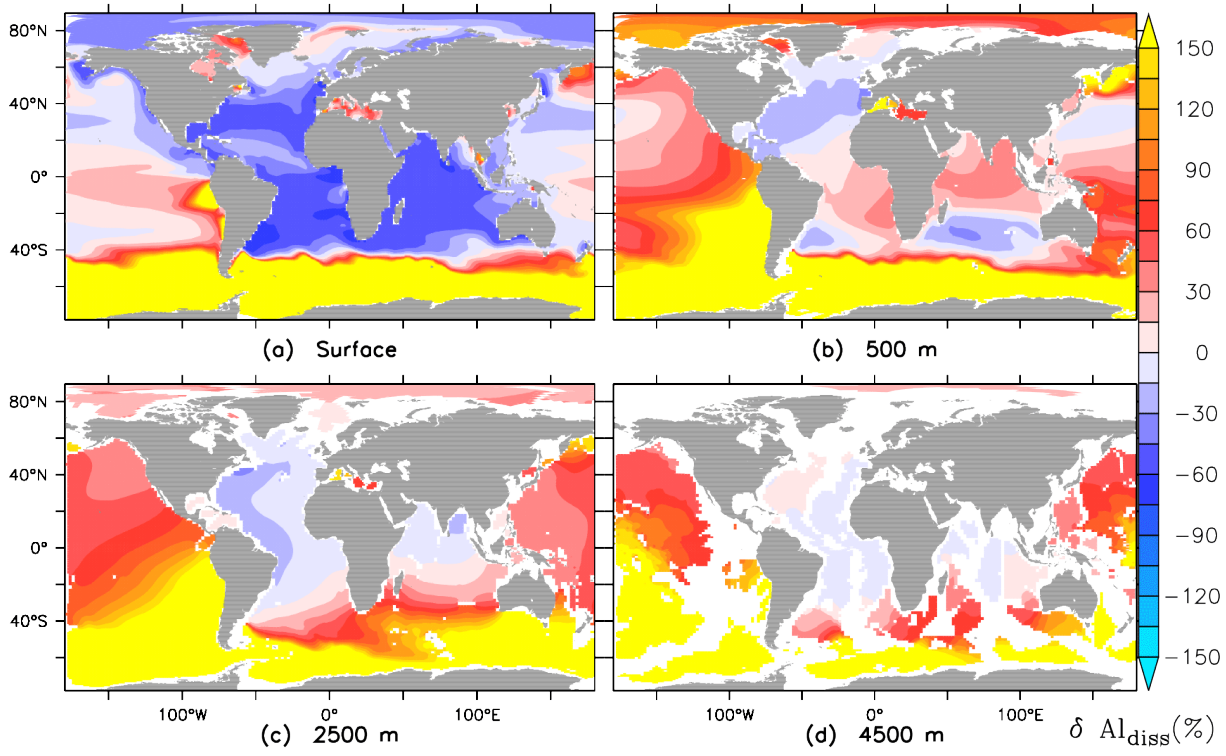

Figure 11. Result of a 500 yr simulation with incorporation (no limitation, i.e. $R_{Al/Si} = [Al_{diss}]/[Si_{diss}]$) and a decreased scavenging partition coefficient $k'_d = k_d/4 = 28 \times 10^3$ dm^3 mol^{-1} (IncorpLowScav). Relative difference of $[Al_{diss}]$ between IncorpLowScav and RefDyn2.

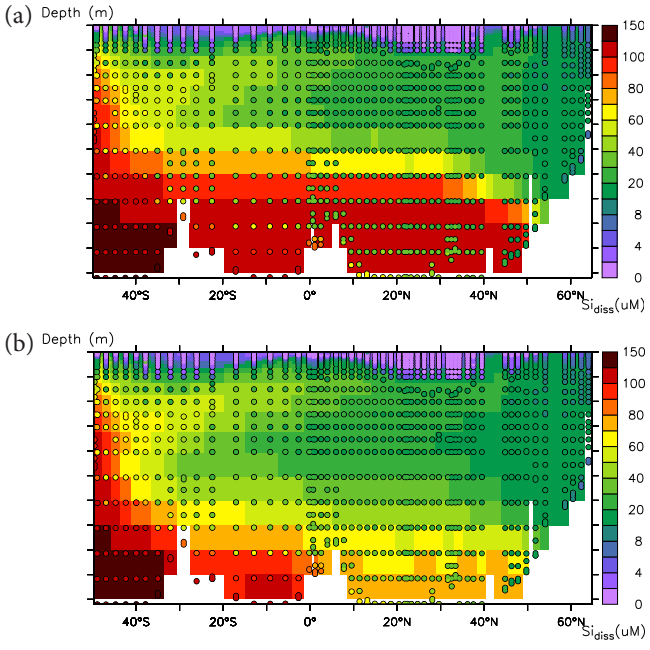

Figure 12. The modelled silicic acid concentration at the West Atlantic GEOTRACES section. Coloured dots are measurements (data from K. Bakker, E. van Weerlee, M. Rijkenberg and H. J. W. de Baar). Both simulated and observed concentrations are in µM (on a non-linear scale).

such as silt and clay particles. For this reason, no one-to-one comparison between modelled and measured biogenic silica can be performed; only a qualitative analysis can easily be done. Aumont and Bopp (2006) showed that primary production of diatoms is small in the oligotrophic North Atlantic Ocean, consistent with measurement-derived biogenic silica export (e.g. Sarmiento and Gruber, 2006, Colour Plate 4).

4.1.2 Dust dissolution

Fractions of each of the elements in lithogenic dust particles dissolve in the upper mixed layer, while below the mixed layer the dissolution of the elements from dust is smaller. It is generally assumed that most of the dust is refractory. Therefore, in our model, Al from lithogenic particles is not dissolved below the mixed layer. The neglect of dissolution below the mixed layer is often casually assumed and has been suggested by many studies on Al in the ocean (e.g. Orians and Bruland, 1986; Baker et al., 2006; Buck et al., 2006). However, no explicit observational study has been published on the fate of lithogenic dust particles in the water column below the mixed layer.

One of the sensitivity simulations of Van Hulten et al. (2013) suggests that there is no dissolution below the mixed layer. That simulation, DustWC, included dissolution of dust below the surface layer, while there was no sediment source. DustWC did not perform better compared to their reference experiment, RefDyn1. The impact of the dissolution below the mixed layer had especially an aggravated impact in the West Atlantic Ocean between 500 and 1500 m depth. Hence, there is good reason for excluding water column dissolution of lithogenic Al. The sediment resuspension simulations of this study (SedProp and SedMackin) include a deep source of Al_{diss}. If dissolution below the mixed layer would be added to these simulations, this would probably worsen the Al_{diss} distribution. Hence, there is good reason for excluding water column dissolution of lithogenic Al.

4.1.3 Reversible scavenging

In our model Al_{diss} is reversibly scavenged. This means that Al_{diss} is scavenged and, during downward settling, partly released in the water column. The release is caused by a combination of decreasing Si_{biog} and Al_{diss} (Eqs 2 and 3). At first sight, this release appears necessary to explain the non-zero water column concentrations of Al_{diss}. This is consistent with the notion that Si_{biog} with Al_{ads} follows the MOC and slowly releases Al_{diss}. This can be seen in Fig. 1a and Figs 4 and 8, where [Al_{diss}] shows the "imprint" of the MOC. Still, it is possible that desorption occurs at a slower rate than adsorption, and that desorption hardly depends on the particle concentration (Moran and Moore, 1992).

In the real ocean adsorptive scavengers other than biogenic Si, as well as different "dissolved" Al particles, may play a role. For example, colloidal Al and other colloids facilitate the removal of trace metals like Al (Moran and Moore, 1989; Moran and Buesseler, 1992). However, the fraction of colloidal Al is only 0.2–3.4 % (of the operationally defined filtrate < 0.2 µm Al_{diss} pool), meaning that the removal of Al occurs mainly through direct adsorption, or the colloidal fraction is rapidly turned over (Dammshäuser and Croot, 2012). Either case implies that the model may skip the colloidal fraction and convert Al_{diss} to Al_{ads} in a single step.[1]

4.2 Sediment source

4.2.1 Resuspension versus diffusion

Typically in shallow waters, dissolved iron (Fe) diffuses from the sediment into the water above due to build-up of reduced Fe within sediment pore waters. Van Hulten et al. (2013) performed a simulation with a sediment source of dissolved Al analogous to Fe. However, reduction and subsequent diffusion of Al from sediments does not typically occur. The sediment input simulation in this work is based on sediment resuspension in deep ocean bottom waters instead of upward diffusion across the sediment–water interface.

[1]Furthermore, Moran and Moore (1988a) note that Al has a large truly dissolved fraction, and "will not be removed as effectively [as Th] during the coagulation process." Finally, and also because of these considerations, the data set available now does not distinguish the colloidal from the soluble pool.

The resuspension hypothesis has a stronger observational basis than the diffusion hypothesis. Observations show that there appears to be an Al source from sediments where there is resuspension, e.g. around the Grand Banks (Moran and Moore, 1991). This typically coincides with regions of deep water formation or it occurs around seafloor elevations. When there does not appear to be resuspension, there is generally no source of Al_{diss}. This of course does not exclude the possibility of diffusion of Al out of sediments, but the observations link near-sediment Al elevations to regions of resuspension. Further discussion and references may be found in Middag et al. (2014).

4.2.2 Shortcomings

Sediment resuspension is actually induced by near-sediment turbulence, creating a layer of water above the sediment containing significant amounts of suspended sediment particles. This layer is about 200–1000 m thick and is referred to as the nepheloid layer (Jackson, 2005). Due to the low vertical resolution of the model (bottom layer is up to 500 m thick), it was not possible to parameterise sediment resuspension by means of the turbulence parameters present in the model. Instead, a certain portion of sedimented biogenic silica was redissolved into the bottom model layer. This is hence not a mechanistic model but a simple parameterisation. This is reasonable because the bottom layer thickness is of the same order of magnitude as the nepheloid layer.

There are no observations or good estimates of Al flux from sediment resuspension, and there is no sediment model for Al available. Therefore it is assumed that recently sedimented Al_{ads} is resuspended and subsequently partly dissolved (e.g. Lampitt, 1985; Hwang et al., 2010). Besides Al_{ads} there is another particulate Al tracer present in some of the model simulations, namely Al_{biog}. This is not used here, since Al incorporated into the frustule lattice is harder to dissolve than Al adsorbed onto Si_{biog}. Also, Koning et al. (2007) state that a significant amount of the Al, associated with diatom frustules post-mortem, can be rinsed off and is thus bound to the surface.

4.2.3 Inhibition

The dissolution of Al from resuspended sediments appears to be inhibited by Si_{diss}. This effect has been included in Eq. (9). Here we try to give an extensive qualitative rationale for the hypothesis, while a derivation of the final equation can be found in Appendix A. We believe that the elevation of $[Al_{diss}]$ in bottom waters (Fig. 1a) is due to significant dissolution/desorption from resuspended sediment in part of the Northern Hemisphere, a process apparently inhibited in the Southern Hemisphere. This may be explained by the mirror image distribution of dissolved silicate (Fig. 1b). Namely, the Si_{diss} concentration is very high in the AABW in the Southern Hemisphere and flows as far north as $\sim 40^\circ$ N, albeit somewhat diluted by vertical mixing with overlying NADW that has lower Si_{diss} concentrations. The high concentration of Si_{diss} in bottom waters possibly prevents the dissolution/desorption of Al from sediments. Briefly, in the northernmost part of the transect the DSOW cascades down over the seafloor from $\sim 65^\circ$ N to $\sim 45^\circ$ N, in the process acquiring more and more dissolved Al due to redissolution/desorption from resuspended sediment particles in the bottom nepheloid layer, which is very thick here (Biscaye and Eittreim, 1977; Gross et al., 1988). Indeed, from 65 to 45° N the dissolved Al in the deepest bottom water sample increases from 12 nM at 65° N to 34 nM at 44.8° N (Middag et al., 2014, their Fig. 9). The parallel increase of $[Si_{diss}]$ is slightly more modest from 8 µM at 65° N to 21 µM at 44.8° N. However, somewhere in between 45° N and 40° N the southwards flowing DSOW becomes underlain by the northward extreme of AABW with much higher $[Si_{diss}] \approx$ 45 µM at 39.5° N. There is still significant sediment resuspension based on optical backscatter observations, but no more release of Al, hence Si_{diss} appears to inhibit any further dissolution/desorption of Al from resuspended sediments.

The overall sediment source of Al_{diss} is likely due to a combination of processes (bottom current velocity, resuspension, partial dissolution of clay minerals, partial dissolution of biogenic debris (Si_{biog}, Al_{biog}) and desorption) where porewater chemistry within the sediments likely plays a role as well. However, neither the observations (Fig. 1a) nor the simulation modelling of dissolved Al have the adequate vertical resolution to resolve all these processes. Instead we follow Mackin and Aller (1986) and the derivation in Appendix A.

4.3 Incorporation

4.3.1 Biology

The simulation Incorp resulted in a much too small $[Al_{diss}]$ in the upper 500 m of the ocean, especially below (and downstream of) dust deposition. In this section three possibilities are discussed that may leave open the option of biological incorporation.

Firstly, too much Al might be biologically incorporated into the frustules. A different moderation term $R_{Al/Si}$ would be able to change that. One way is to decrease c_{in}. This parameter describes a general preference of silicic acid above aluminium when it is smaller than one and vice versa. Han et al. (2008) defined $c_{in} = 0.08845$, loosely based on Gehlen et al. (2002). Alternatively, one may also define a maximum incorporation r_{max}. This parameter signifies that diatoms do not allow aluminium in their frustule above a certain percentage. Several equivocal values for r_{max} may be derived from different studies, among which are 0.007, based on Gehlen et al. (2002) as well, or 0.01 (van Cappellen et al., 2002), or 0.0022, an incorporation ratio based on observations of $[Al_{diss}]$ and $[Si_{diss}]$ at remineralisation depth (Middag et al.,

2009). An additional simulation was performed with the parameterisation by Han et al. (2008), i.e. with $c_{in} = 0.08845$ and $r_{max} = \infty$ (results not presented here). This simulation does not yield significant changes compared to the reference simulation (RefDyn2). Hence, from these simulations it cannot be concluded whether incorporation (with a reduced incorporation rate c_{in}) occurs.

Secondly, whether incorporation is moderated or not, the part of the model that is independent of incorporation is likely to need retuning, since incorporation functions as an extra sink of Al. The settling velocity w_s scavenging parameters k_d and κ may need to be adjusted (see Eqs. 2, 3 and 6). For instance, the partition coefficient k_d may be decreased. This leaves more Al_{diss} in the surface ocean, compensating the decrease of $[Al_{diss}]$ by incorporation. To test this hypothesis a simulation was performed with incorporation and a decreased k_d (IncorpLowScav). This simulation showed a large effect of k_d on the Southern Ocean, and not on the Atlantic Ocean, where incorporation had such a large effect (Sect. 3.4). Why is this the case?

In our model, in chemical equilibrium, the adsorbed Al concentration is proportional to both $[Al_{diss}]$ and $[Si_{biog}]$ (Eq. 3). The effect of the biogenic Si dependence is evident in high-$[Si_{biog}]$ areas like the Southern Ocean. Furthermore, Si_{biog} is present in and below the euphotic zone, especially in the Southern Ocean. This results in scavenging throughout a significant portion of the water column. In other words, k_d has a much stronger sensitivity in the polar oceans compared to other locations, as is actually shown by a simulation of Van Hulten et al. (2013). A smaller k_d therefore results in more Al_{diss} in the Southern Ocean, while it has little effect on the more problematic incorporation-induced decrease of $[Al_{diss}]$ in the Atlantic Ocean.

Increasing dust deposition, or solubility, is another possibility to compensate the decrease of $[Al_{diss}]$ in the main thermocline in the simulations where biological incorporation occurs. A preliminary simulation suggests that more dust only affects the very surface of the ocean. Dust deposition and dissolution of Al in the surface layer does not affect the subsurface $[Al_{diss}]$ much (at 50–400 m depth), while as a consequence of biological incorporation a strong depletion of Al_{diss} occurs there as well (result not presented here). Dissolving lithogenic dust particles below the ocean surface is another option. This has been done in Van Hulten et al. (2013) by means of instantaneous dissolution in the water column upon deposition on the sea surface according to a function that exponentially decreases with depth. The depth-dependent dissolution function can be fitted to the observations or the reference simulation, giving a reasonable first-order simulation of $[Al_{diss}]$. Obviously, a simulation with incorporation and a dissolution function fitted to the observations is not very strong evidence for incorporation.

To summarise, the simulation IncorpLowScav showed that changing k_d cannot solve the problem, and we have to understand why this is the case. Also a simulation with increased dust dissolution does not give much hope. This suggests that biological incorporation of Al into diatoms has only a second-order effect on the dissolved Al distribution. This is in line with the likely overestimation of Al to Si ratio in our model during incorporation as discussed near the beginning of this section. Indeed, there are several studies that cannot detect the process of biological incorporation of Al into living diatoms (e.g. Vrieling et al., 1999) and many studies are unclear about the actual mechanism of removal (e.g. Moran and Moore, 1988a; Ren et al., 2011). However, as discussed, at the same time there are many studies strongly suggesting the biological incorporation. Either parts of the model (which is of relatively large complexity and contains many degrees of freedom) are overlooked, e.g. in the complexities of the Si cycle; or the amount of incorporation is smaller than assumed in Incorp.

4.3.2 Post-mortem diagenesis within the sediments

Koning et al. (2007) and Loucaides et al. (2012, 2010) have suggested that most of the Al found in diatom silicate in sediments is incorporated after burial. These papers indicate that the Al / Si ratio in living diatoms is most likely considerably lower than the estimates used in the incorporation simulations. Most incorporation is indeed after burial and hence post-mortem. However, sedimentary processes are not the focus of this work and only matters are discussed that are of direct importance for the processes in the water column. What we aimed for here is to test the effect on $[Al_{diss}]$ by including biological incorporation in opal of growing diatoms by using the upper limit of Al / Si (namely the ambient dissolved Al / Si concentration ratio in the surface ocean waters). A study on sedimentary processes is beyond the scope of this paper.

5 Conclusions

The Al_{diss} distribution in the upper part of the ocean has previously been simulated reasonably well with only a dust source and reversible scavenging as the removal process (Van Hulten et al., 2013). However, the $[Al_{diss}]$ was strongly underestimated in the deep North Atlantic Ocean, highlighting deficiencies in this model. The simulation is significantly improved by the use of different dynamical fields and the addition of a resuspension source. The latter supports the idea that the most significant sources of Al to the ocean are dust deposition and sediment resuspension, and the most important internal process is likely to be adsorptive scavenging. The Al release from resuspended sediment appears to depend on both Al_{ads} sedimentation and bottom water $[Si_{diss}]$. It has been shown that a parameterisation based on Mackin and Aller (1986) is able to simulate the deep ocean $[Al_{diss}]$ realistically, supporting the idea of stoichiometric saturation. This implies that Al release from resuspension occurs only

in bottom waters with relatively low Si_{diss}. These waters are in the northern North Atlantic Ocean and the Arctic Ocean (Middag et al., 2009); all other ocean basins have high Si_{diss} in bottom waters that prevents such Al release. In fact, within the Arctic Ocean, indeed in bottom waters, there is an elevated trend of the dissolved Al / Si ratio as compared to mid-waters, i.e. an indication of extra release of Al (Middag et al., 2009, their Figs 5, 8, 13 and 18).

A data set of measurements of $[Al_{diss}]$ in the deep and bottom waters has been used, much larger than hitherto available. Nevertheless, the vertical resolution near the deep ocean seafloor still is modest. Similarly, the deepest bottom water box of the model extends to 500 m above the seafloor, and in some regions the model extent of 5000 m is less than the true full water column depth. Obviously, the very intriguing sediment source of Al in the 40 to 65° N region would be of great interest for a more detailed study with high vertical resolution sampling just above the seafloor and similar high vertical resolution modelling. Also porewater dynamics is potentially important, hence it may be necessary to include a more detailed parameterisation in future models. Similarly, other types of particulate Al in resuspended sediments should be considered in modelling.

Simulations with biological incorporation show that this process is unlikely to occur proportional to the ambient dissolved Al / Si concentration ratio. The simulations suggest that the relative importance of incorporation compared to scavenging may be small, because changing the scavenging parameters or surface dust dissolution cannot compensate for the unrealistic decrease of dissolved Al in the main thermocline. This does not imply that incorporation does not take place, yet perhaps net incorporation is relatively small.

Clearly, more simulations, laboratory experiments and field observations are needed to answer what the relative amount of incorporation is compared to scavenging. When a realistic model of incorporation has been developed, the next step is to test the effect of Al on the Si cycle which could finally shed light on how large this effect is for the world ocean and the role of diatoms in the climate system.

Finally, a word of caution. On the one hand, the resulting overall improved simulation or fit versus the measurements of $[Al_{diss}]$ and $[Si_{diss}]$ is another step forward. On the other hand, for such a complex circulation–biogeochemistry model with so many parameterisations, one cannot exclude the possibility of other combinations of parameterisations resulting in a similar or perhaps even better goodness of fit to the measurements. In other words, while the chosen processes of Al supply and Al removal are sensible, also in keeping with views in the literature, as is the ensuing fair simulation, the findings should not be overinterpreted as conclusive evidence in support of the chosen processes and their parameterisation.

Appendix A: Sediment resuspension model

Based on observations, Mackin and Aller (1986) hypothesised that release of Al from sediment is inhibited by porewater silicic acid, $Si(OH)_4$. They wrote the following, using { } for chemical activity and p for $-\log_{10}$ as also in pH:

> In general, when stoichiometric saturation (sensu Thorstenson and Plummer (1977)) exists for an authigenic clay of constant composition in sediment porewater having nearly invariant reactive cation concentrations, the following will hold (Mackin and Aller, 1984):
>
> $$p\{Al(OH)_4^-\} + ap\{Si(OH)_4\} + b\,\mathrm{pH} = pK_{eq}, \quad \text{(A1)}$$
>
> where [$a = Si/Al$ and $b = H^+/Al$ are the stoichiometries] of the clay and pK_{eq} = apparent constant excluding the effects of major cations and other potentially reactive cations. To estimate values of a and b for the Amazon shelf sediments from [their] Fig. 2, we applied a regression technique which treats $p\{Al(OH)_4^-\}$, $p\{Si(OH)_4\}$ and pH as independent variables (Mackin and Aller, 1984). The results of this treatment give the following:
>
> $$1(\pm 0.044)\,p\{Al(OH)_4^-\} + 0.828(\pm 0.093)\quad \text{(A2)}$$
> $$p\{Si(OH)_4\} + 0.429(\pm 0.070)\mathrm{pH} = pK_{eq},$$
>
> where $pK_{eq} = 13.98(\pm 0.13)$.

The chemical activities are in nM and µM for $Al(OH)_4^-$ and $Si(OH)_4$, respectively. Their use of stoichiometric saturation is consistent with the mirror image between $[Al(OH)_4^-]$ and $[Si(OH)_4]$ as shown in Fig. 1. Here $[Al(OH)_4^-]_{bottom}$ is small in the Southern Hemisphere and large in the Northern Hemisphere, while both south of 40° S and north of 40° N sediment particles are present in the bottom water (Fig. 2), strongly suggesting sediment resuspension. Actually, just south of 40° N is the largest sediment resuspension, even though just north of this latitude, $[Al_{diss}]$ is mostly elevated near the sediment.

Eq. (A1) can be rewritten as

$$\log_{10}\{Al_{diss}\}_{pore} + a \cdot \log_{10}\{Si_{diss}\}_{pore} = B, \quad \text{(A3)}$$

where $Al_{diss} = Al(OH)_4^-$, $Si_{diss} = Si(OH)_4$, and with $B = b\mathrm{pH} - pK_{eq}$ being an approximate constant (for pH = 8.1, $B = -10.5$). The dissolved entities between the curly braces are chemical activities in the porewater, but we need to model fluxes from resuspended sediment into bottom water. We will refer to the model layer (of max. 500 m thick) just above the sediment as *bottom water*.

Since $[Al_{diss}]$ and $[Si_{diss}]$ are high in porewater (at least $[Si_{diss}]$ is very high in Southern Ocean porewater), the chemical activities are not equal to the concentrations. But they are proportional; their coefficients of proportionality are the activity coefficients γ_{Al} and γ_{Si} (e.g. Stone and Morgan, 1990):

$$\begin{aligned}\{Al_{diss}\}_{pore} &= \gamma_{Al}[Al_{diss}]_{pore}\\ \{Si_{diss}\}_{pore} &= \gamma_{Si}[Si_{diss}]_{pore}\,.\end{aligned} \quad \text{(A4)}$$

So far we have rewritten the equations of Mackin and Aller (1986) using simple mathematics and chemistry. We will now introduce the model. For this purpose we will assume that the empirical relationship of Mackin and Aller (1986) (Eq. A1), found at the Amazon shelf, is valid everywhere. This assumption is defendable if Mackin and Aller (1986) have not made any extra implicit assumptions on top of the research of Thorstenson and Plummer (1977); the latter only used established thermodynamical relations.

From Eqs (A3) and (A4) the following relation can be derived:

$$\log_{10}(\gamma_{Al}[Al_{diss}]_{pore}) = B - a \cdot \log_{10}(\gamma_{Si}[Si_{diss}]_{pore}) \quad \text{(A5)}$$
$$\begin{aligned}[Al_{diss}]_{pore}/\mathrm{nM} &= \frac{10^B}{\gamma_{Al}} \cdot \left(\gamma_{Si}[Si_{diss}]_{pore}/\mu M\right)^{-a}\\ &= C \cdot ([Si_{diss}]_{pore}/\mu M)^{-a},\end{aligned}$$

where $C = 10^B \gamma_{Al}^{-1} \gamma_{Si}^{-a} > 0$.

The Al flux Φ_{sed} from the bottom water layer to the sediment is given by $\Phi_{sed} = w_s \cdot [Al_{ads}]$, with $[Al_{ads}]$ the bottom water layer concentration of adsorbed Al and w_s the sedimentation rate. In line with the sediment resuspension hypothesis, we assume that the aluminium flux Φ_{resusp} from resuspension and subsequent release of Al_{diss} (henceforth *resuspension flux*) is proportional to Φ_{sed}, converting part of the sedimented Al into dissolved Al in the bottom water layer:

$$\Phi_{resusp} = \beta \cdot \Phi_{sed} = \beta \cdot w_s \cdot [Al_{ads}], \quad \text{(A6)}$$

where $\beta \in [0, 1]$ is the fraction of resuspended and subsequently released Al. In the original resuspension model, β is a constant. In the more complex model, the resuspension flux is taken to be proportional to $[Al_{diss}]_{pore}$ (as well as $[Al_{ads}]$). Using Eq. (A5), this results in

$$\beta \propto [Al_{diss}]_{pore}/\mathrm{nM} \propto ([Si_{diss}]_{pore}/\mu M)^{-a}\,. \quad \text{(A7)}$$

Furthermore, we assume that bottom water $[Si_{diss}]$ is proportional to porewater $[Si_{diss}]$. It is a first-order assumption. Since we lack the knowledge of whether this is reasonable, it would be useful if this assumption were tested, but that is far beyond the scope of this work. Therefore, we cannot give an explanation or perform a mechanistic simulation. Together with Eqs (A6) and (A7), this assumption gives for the change of $[Al_{diss}]$ in the bottom layer due to resuspension:

$$\begin{aligned}\left.\frac{\partial [Al_{diss}]}{\partial t}\right|_{resusp} &= \frac{\Phi_{resusp}}{\Delta z_{bottom}} = \beta \cdot \frac{\Phi_{sed}}{\Delta z_{bottom}}\\ &= \beta_0 \left(\frac{[Si_{diss}]_{bottom}}{\mu M}\right)^{-a} \cdot \frac{\Phi_{sed}}{\Delta z_{bottom}},\end{aligned} \quad \text{(A8)}$$

where β_0 is a dimensionless constant and Δz_{bottom} is the thickness of the bottom seawater model layer.

Since there can be no more redissolution than the amount of Al that sediments (assuming steady state and no horizontal remobilisation of sediment), β is at most one. If we want to use the highest possible flux for resuspension near 45–50° N, we set $\beta = 1$ in that region. The modelled bottom water $[\text{Si}_{\text{diss}}]$ near 50° N is 30.3 µM. Hence, the proportionality constant is $\beta_0 = 30.3^{0.828} = 16.85$. Since bottom $[\text{Si}_{\text{diss}}]$ farther north is lower, β would there be higher than one. Since the model assumes that only recently sedimented Al_{ads} is resuspended, it would not be physically correct if $\beta > 1$. Therefore β is constrained and hence given by

$$\beta = \min(16.85 \cdot ([\text{Si}_{\text{diss}}]/\mu\text{M})^{-0.828}, 1)\ , \tag{A9}$$

which is to be plugged into the concentration change:

$$\frac{\partial[\text{Al}_{\text{diss}}]}{\partial t}\Big|_{\text{resusp}} = \beta \cdot \frac{\Phi_{\text{sed}}}{\Delta z_{\text{bottom}}}\ . \tag{A10}$$

This equation is identical to Eq. (8) in the main text, hence this result is what was to be demonstrated.

As a sanity check we substitute the minimum (13.4 µM) and the maximum (148.6 µM) bottom $[\text{Si}_{\text{diss}}]$ into this equation:

$$\begin{aligned}\beta_{\max} &= \min(16.85 \cdot 13.4^{-0.828}, 1) \\ &= \min(1.96, 1) = 1\end{aligned} \tag{A11}$$

$$\beta_{\min} = \min(16.85 \cdot 148.6^{-0.828}, 1) = 0.27 \tag{A12}$$

This means that since bottom $[\text{Si}_{\text{diss}}]$ is decreasing with latitude, we expect 100 % redissolution anywhere north of 45° N (it is set up like that). About 25 % of the sedimenting Al_{ads} is dissolved in the Southern Ocean.

The Supplement related to this article is available online at doi:10.5194/bg-11-3757-2014-supplement.

Acknowledgements. The authors are grateful to those who have been proved useful in discussion, including Justus van Beusekom, Tom Remenyi, Micha Rijkenberg, Wilco Hazeleger and our colleagues from the IMAU Institute. We also want to thank Christoph Heinze, Phoebe Lam and Andreas Schmittner for providing their data. The authors wish to acknowledge the use of the free software visualisation and analysis programs Ferret and R. Other noteworthy libre software used is the GNU Operating System and Climate Data Operators. Useful tips for statistical analysis were provided by several colleagues, notably Ronald van Haren and Carlo Lacagnina. We would also like to thank the three reviewers (two anonymous and Justus van Beusekom) as well as the editor for their suggestions for improving the paper. This research is funded by the Netherlands Organisation for Scientific Research (NWO), grant no. 839.08.414, part of the ZKO programme.

Edited by: C. P. Slomp

References

Arsouze, T., Dutay, J.-C., Lacan, F., and Jeandel, C.: Reconstructing the Nd oceanic cycle using a coupled dynamical–biogeochemical model, Biogeosciences, 6, 2829–2846, doi:10.5194/bg-6-2829-2009, 2009.

Aumont, O. and Bopp, L.: Globalizing results from ocean in situ iron fertilization studies, Global Biogeochem. Cy., 20, GB2017, doi:10.1029/2005GB002591, 2006.

Baker, A., Jickells, T., Witt, M., and Linge, K.: Trends in the solubility of iron, aluminium, manganese and phosphorus in aerosol collected over the Atlantic Ocean, Mar. Chem., 98, 43–58, 2006.

Behrenfeld, M., O'Malley, R., Siegel, D., McClain, C., Sarmiento, J., Feldman, G., Milligan, A., Falkowski, P., Letelier, R., and Boss, E.: Climate-driven trends in contemporary ocean productivity, Nature, 444, 752–755, 2006.

Biscaye, P. and Eittreim, S.: Suspended particulate loads and transports in the nepheloid layer of the abyssal Atlantic Ocean, Mar. Geol., 23, 155–172, 1977.

Brodeau, L., Barnier, B., Treguier, A.-M., Penduff, T., and Gulev, S.: An ERA40-based atmospheric forcing for global ocean circulation models, Ocean Model., 31, 88–104, 2010.

Brown, M. and Bruland, K.: Dissolved and particulate aluminum in the Columbia River and coastal waters of Oregon and Washington: Behavior in near-field and far-field plumes, Estuar. Coast. Shelf S., 84, 171–185, 2009.

Brown, M., Lippiatt, S., and Bruland, K.: Dissolved aluminum, particulate aluminum, and silicic acid in northern Gulf of Alaska coastal waters: Glacial/riverine inputs and extreme reactivity, Mar. Chem., 122, 160–175, 2010.

Buck, C., Landing, W., Resing, J., and Lebon, G.: Aerosol iron and aluminum solubility in the northwest Pacific Ocean: Results from the 2002 IOC cruise, Geochem. Geophy. Geosy., 7, Q04M07, doi:10.1029/2005GC000977, 2006.

Chou, L. and Wollast, R.: Biogeochemical behavior and mass balance of dissolved aluminum in the western Mediterranean Sea, Deep-Sea Res. Part II, 44, 741–768, doi:10.1016/S0967-0645(96)00092-6, 1997.

Dammshäuser, A. and Croot, P.: Low colloidal associations of aluminium and titanium in surface waters of the tropical Atlantic, Geochim. Cosmochim. Ac., 96, 304–318, doi:10.1016/j.gca.2012.07.032, 2012.

de Jong J., Boyé, M., Gelado-Caballero, M., Timmermans, K., Veldhuis, M., Nolting, R., van den Berg, C., and de Baar, H.: Inputs of iron, manganese and aluminium to surface waters of the Northeast Atlantic Ocean and the European continental shelf, Mar. Chem., 107, 120–142, 2007.

Dixit, S., Van Cappellen, P., and van Bennekom, A.: Processes controlling solubility of biogenic silica and pore water build-up of silicic acid in marine sediments, Mar. Chem., 73, 333–352, 2001.

Dutay, J., Lacan, F., Roy-Barman, M., and Bopp, L.: Influence of particle size and type on ^{231}Pa and ^{230}Th simulation with a global coupled biogeochemical-ocean general circulation model: A first approach, Geochim. Geochem. Geophy., 10, Q01011, doi:10.1029/2008GC002291, 2009.

Elderfield, H. and Schultz, A.: Mid-ocean ridge hydrothermal fluxes and the chemical composition of the ocean, Ann. Rev. Earth Planet. Sci., 24, 191–224, 1996.

Ethé, C., Aumont, O., Foujols, M.-A., and Lévy, M.: NEMO reference manual, tracer component : NEMO-TOP. Preliminary version, Note du Pole de Modélisation, Institut Pierre-Simon Laplace, 2006.

Gehlen, M., Beck, L., Calas, G., Flank, A., BennekomVanA.J.van, and BeusekomVanJ.E.E.van: Unraveling the atomic structure of biogenic silica: evidence of the structural association of Al and Si in diatom frustules, Geochim. Cosmochim. Ac., 66, 1601–1609, 2002.

Gehlen, M., Heinze, C., Maier-Reimer, E., and Measures, C.: Coupled Al-Si geochemistry in an ocean general circulation model: A tool for the validation of oceanic dust deposition fields?, Global Biogeochem. Cy., 17, 1028, doi:10.1029/2001GB001549, 2003.

Gehlen, M., Gangstø, R., Schneider, B., Bopp, L., Aumont, O., and Ethe, C.: The fate of pelagic $CaCO_3$ production in a high CO_2 ocean: a model study, Biogeosciences, 4, 505–519, doi:10.5194/bg-4-505-2007, 2007.

Gross, T. F., Williams, A., and Newell, A.: A deep-sea sediment transport storm, Nature, pp. 518–521, doi:10.1038/331518a0, 1988.

Han, Q., Moore, J., Zender, C., and Hydes, D.: Constraining oceanic dust deposition using surface ocean dissolved Al, Global Biogeochem. Cy., 22, GB2038, doi:10.1029/2007GB002975, 2008.

Han, Q., Zender, C., Moore, J., Buck, C., Chen, Y., Johansen, A., and Measures, C.: Global estimates of mineral dust aerosol iron and aluminum solubility that account for particle size using diffusion-controlled and surface-area-controlled approximations, Global Biogeochem. Cy., 26, GB2038, doi:10.1029/2011GB004186, 2012.

Hauglustaine, D., Hourdin, F., Jourdain, L., Filiberti, M.-A., Walters, S., Lamarque, J.-F., and Holland, E.: Interactive chemistry in the Laboratoire de Météorologie Dynamique general circulation model: Description and background tropospheric chemistry evaluation, J. Geophys. Res.: Atmospheres, 109, D04314, doi:10.1029/2003JD003957, 2004.

Hwang, J., Druffel, E. R., and Eglinton, T.: Widespread influence of resuspended sediments on oceanic particulate organic carbon: Insights from radiocarbon and aluminum contents in sinking particles, Global Biogeochem. Cy., 24, GB4016, doi:10.1029/2010GB003802, 2010.

Hydes, D., Statham, P., and Burton, J.: A vertical profile of dissolved trace metals (Al, Cd, Cu, Mn, Ni) over the median valley of the mid Atlantic ridge, 43° N: Implications for Hydrothermal activity, Sci. Total Environ., 49, 133–145, 1986.

Hydes, D., de Lange, G., and BaarDeH.J.W.de: Dissolved aluminium in the Mediterranean, Geochim. Cosmochim. Ac., 52, 2107–2114, 1988.

Jackson, J.: Glossary of geology, Springer, Berlin, 5th revised and enlarged Edn., 2005.

Jickells, T., An, Z., Andersen, K., Baker, A., Bergametti, G., Brooks, N., Cao, J., Boyd, P., Duce, R., Hunter, K., Kawahata, H., Kubilay, N., de la Roche, J., Liss, P., Mahowald, N., Prospero, J., Ridgwell, A., Tegen, I., and Torres, R.: Global iron connections between desert dust, ocean biogeochemistry, and climate, Science, 308, 67–71, 2005.

Jones, M., Pearce, C., and Oelkers, E.: An experimental study of the interaction of basaltic riverine particulate material and seawater, Geochim. Cosmochim. Ac., 77, 108–120, 2012.

Koning, E., Gehlen, M., Flank, A.-M., Calas, G., and Epping, E.: Rapid post-mortem incorporation of aluminum in diatom frustules: Evidence from chemical and structural analyses, Mar. Chem., 106, 208–222, 2007.

Kramer, J., Laan, P., Sarthou, G., Timmermans, K., and De Baar, H.: Distribution of dissolved aluminium in the high atmospheric input region of the subtropical waters of the North Atlantic Ocean, Mar. Chem., 88, 85–101, 2004.

Kremling, K.: The distribution of cadmium, copper, nickel, manganese, and aluminium in surface waters of the open Atlantic and European shelf area, Deep-Sea Res. Pt A, 32, 531–555, 1985.

Lam, P.: The dynamic ocean biological pump: Insights from a global compilation of particulate organic carbon, CaCO3, and opal concentration profiles from the mesopelagic, Global Biogeochem. Cy., 25, GB3009, doi:10.1029/2010GB003868, 2011.

Lampitt, R.: Evidence for the seasonal deposition of detritus to the deep-sea floor and its subsequent resuspension, Deep-Sea Res. Pt. A, 32, 885–897, 1985.

Large, W. and Yeager, S.: Diurnal to decadal global forcing for ocean and sea-ice models: The data sets and flux climatologies, National Center for Atmospheric Research, 2004.

Lewin, J.: The dissolution of silica from diatom walls, Geochim. Cosmochim. Ac., 21, 182–198, 1961.

Loucaides, S., Behrends, T., and van Cappellen, P.: Reactivity of biogenic silica: Surface versus bulk charge density, Geochim. Cosmochim. Ac., 74, 517–530, 2010.

Loucaides, S., Koning, E., and Van Cappellen, P.: Effect of pressure on silica solubility of diatom frustules in the oceans: Results from long-term laboratory and field incubations, Mar. Chem., 136, 1–6, 2012.

Lunel, T., Rudnicki, M., Elderfield, H., and Hydes, D.: Aluminium as a depth-sensitive tracer of entrainment in submarine hydrothermal plumes, Nature, 344, 137–139, 1990.

Mackin, J.: Control of dissolved Al distributions in marine sediments by clay reconstitution reactions: experimental evidence leading to a unified theory, Geochim. Cosmochim. Ac., 50, 207–214, 1986.

Mackin, J. and Aller, R.: Dissolved Al in sediments and waters of the East China Sea: implications for authigenic mineral formation, Geochim. Cosmochim. Ac., 48, 281–297, 1984.

Mackin, J. and Aller, R.: The effects of clay mineral reactions on dissolved Al distributions in sediments and waters of the Amazon continental shelf, Cont. Shelf Res., 6, 245–262, 1986.

Madec, G.: NEMO ocean engine, Note du Pole de Modélisation, Institut Pierre-Simon Laplace, 2008.

Madec, G., Delecluse, P., Imbard, M., and Lévy, C.: OPA 8.1 Ocean General Circulation Model reference manual, Note du Pole de Modélisation, Institut Pierre-Simon Laplace, 11, 91 pp., http://hal.archives-ouvertes.fr/hal-00154217/en/, 1998.

Maier-Reimer, E.: Geochemical cycles in an ocean general circulation model. Preindustrial tracer distributions, Global Biogeochem. Cy., 7, 645–677, 1993.

Maring, H. and Duce, R.: The impact of atmospheric aerosols on trace metal chemistry in open ocean surface seawater, 1. Aluminum, Earth Planet Sc. Lett., 84, 381–392, 1987.

Middag, R.: Dissolved Aluminium and Manganese in the Polar Oceans, Ph.D. thesis, University of Groningen, 2010.

Middag, R., de Baar, H., Laan, P., and Bakker, K.: Dissolved aluminium and the silicon cycle in the Arctic Ocean, Mar. Chem., 115, 176–195, 2009.

Middag, R., de Baar, H., Laan, P., Cai, P., and van Ooijen, J.: Dissolved manganese in the Atlantic sector of the Southern Ocean, Deep-Sea Res. Pt. II, 58, 2661–2677, 2011a.

Middag, R., van Slooten, C., de Baar, H., and Laan, P.: Dissolved aluminium in the Southern Ocean, Deep-Sea Res. Pt. II, 58, 2647–2660, 2011b.

Middag, R., de Baar, H., Laan, P., and Huhn, O.: The effects of continental margins and water mass circulation on the distribution of dissolved aluminum and manganese in Drake Passage, J. Geophys. Res., 117, C01019, doi:10.1029/2011JC007434, 2012.

Middag, R., de Baar, H., Klunder, M., and Laan, P.: Fluxes of dissolved aluminum and manganese to the Weddell Sea and indications for manganese co-limitation, Limnol. Oceanogr., 58, 287–300, 2013.

Middag, R., van Hulten, M. M. P., van Aken, H., Rijkenberg, M., Gerringa, L. J. A., Laan, P., and de Baar, H. J. W.: Aluminium in the ocean: unique mirror image of the biological cycle, submitted, Mar. Chem., 2014.

Moore, J. and Braucher, O.: Sedimentary and mineral dust sources of dissolved iron to the world ocean, Biogeosciences, 5, 631–656, 2008, http://www.biogeosciences.net/5/631/2008/.

Moran, S. and Buesseler, K.: Short residence time of colloids in the upper ocean estimated from 238U–234Th disequilibria, 1992.

Moran, S. and Moore, R.: Evidence from mesocosm studies for biological removal of dissolved aluminium from sea water, Nature, 335, 706–708, 1988a.

Moran, S. and Moore, R.: Temporal variations in dissolved and particulate aluminum during a spring bloom, Estuar. Coast. Shelf S., 27, 205–215, 1988b.

Moran, S. and Moore, R.: The distribution of colloidal aluminum and organic carbon in coastal and open ocean waters off Nova Scotia, Geochim. Cosmochim. Ac., 53, 2519–2527, 1989.

Moran, S. and Moore, R.: The potential source of dissolved aluminum from resuspended sediments to the North Atlantic Deep Water, Geochim. Cosmochim. Ac., 55, 2745–2751, 1991.

Moran, S. and Moore, R.: Kinetics of the removal of dissolved aluminum by diatoms in seawater: A comparison with thorium, Geochim. Cosmochim. Ac., 56, 3365–3374, 1992.

Moran, S., Moore, R., and Westerlund, S.: Dissolved aluminum in the Weddell Sea, Deep-Sea Res. Pt. A, 39, 537–547, 1992.

Nelson, D., Tréguer, P., Brzezinski, M., Leynaert, A., and Quéguiner, B.: Production and dissolution of biogenic silica in the ocean: revised global estimates, comparison with regional data and relationship to biogenic sedimentation, Global Biogeochem. Cy., 9, 359–359, 1995.

Obata, H., Alibo, D., and Nozaki, Y.: Dissolved aluminum, indium, and cerium in the Sea of Japan and the Sea of Okhotsk: Comparison to the marginal seas of the western North Pacific, J. Geophys. Res., 112, C12003, doi:10.1029/2006JC003944, 2007.

Orians, K. and Bruland, K.: The biogeochemistry of aluminum in the Pacific Ocean, Earth Planet Sc. Lett., 78, 397–410, 1986.

Rayner, D., Hirschi, J.-M., Kanzow, T., Johns, W., Wright, P., Frajka-Williams, E., Bryden, H., Meinen, C., Baringer, M., Marotzke, J., et al.: Monitoring the Atlantic meridional overturning circulation, Deep-Sea Res. Pt II, 58, 1744–1753, 2011.

Remenyi, T.: Investigating the impact of aeolian deposition to the Southern Ocean using dissolved aluminium concentrations, Doctor of philosophy in quantitative marine science, Quantitative Marine Science Program, UTas and CSIRO joint program., 2013.

Ren, J.-L., Zhang, G.-L., Zhang, J., Shi, J.-H., Liu, S.-M., Li, F.-M., Jin, J., and Liu, C.-G.: Distribution of dissolved aluminum in the Southern Yellow Sea: Influences of a dust storm and the spring bloom, Mar. Chem., 125, 69–81, 2011.

Sarmiento, J. and Gruber, N.: Ocean Biogeochemical Dynamics, Princeton University Press, 2006.

Slemons, L., Murray, J., Resing, J., Paul, B., and Dutrieux, P.: Western Pacific coastal sources of iron, manganese, and aluminum to the Equatorial Undercurrent, Global Biogeochem. Cy., 24, GB3024, doi:10.1029/2009GB003693, 2010.

Stoffyn, M.: Biological control of dissolved aluminum in seawater: experimental evidence, Science, 203, 651, doi:10.1126/science.203.4381.651, 1979.

Stoffyn, M. and Mackenzie, F.: Fate of dissolved aluminum in the oceans, Mar. Chem., 11, 105–127, 1982.

Stone, A. and Morgan, J.: Kinetics of Chemical Transformation in the Environment, in: Aquatic chemical kinetics: reaction rates of processes in natural waters, edited by: Stumm, W., John Wiley and Sons, vol. 2, chap. 1, 1–42, 1990.

Stow, C., Jolliff, J., Jr., D. M., Doney, S., Allen, J., Friedrichs, M., Rose, K., and Wallhead, P.: Skill assessment for coupled biological/physical models of marine systems, J. Marine Syst., 76, 4–15, 2009.

Tagliabue, A., Bopp, L., Dutay, J.-C., Bowie, A., Chever, F., Jean-Baptiste, P., Bucciarelli, E., Lannuzel, D., Remenyi, T., Sarthou, G., Aumont, O., Gehlen, M., and Jeandel, C.: Hydrothermal contribution to the oceanic dissolved iron inventory, Nat. Geosci., 3, 252–256, 2010.

Talley, L., Reid, J., and Robbins, P.: Data-based meridional overturning streamfunctions for the global ocean, J. Climate, 16, 3213–3226, 2003.

Textor, C., Schulz, M., Guibert, S., Kinne, S., Balkanski, Y., Bauer, S., Berntsen, T., Berglen, T., Boucher, O., Chin, M., et al.: Analysis and quantification of the diversities of aerosol life cycles within AeroCom, Atmos. Chem. Phys, 6, 1777, doi:10.5194/acp-6-1777-2006, 2006.

Thorstenson, D. and Plummer, L.: Equilibrium criteria for two-component solids reacting with fixed composition in an aqueous phase; example, the magnesian calcites, Am. J. Sci., 277, 1203–1223, 1977.

Tréguer, P. and De La Rocha, C.: The World Ocean Silica Cycle, Ann. Rev. Mar. Sci., 5, 477–501, doi:10.1146/annurev-marine-121211-172346, 2013.

Uppala, S.M., Kållberg, P.W., Simmons, A.J., Andrae, U., Bechtold, V., Fiorino, M., Gibson, J.K., Haseler, J.K., Hernandez, A., Kelly, G.A., Li, X., Onogi, K., Saarinen, S., Sokka, N., Allan, R. P., Andersson, E., Arpe, K., Balmaseda, M. A., Beljaars, A. C. M., Berg, L. Van De, Bidlot, J., Bormann, N., Caires, S., Chevallier, F., Dethof, A., Dragosavac, M., Fisher, M., Fuentes, M., Hagemann, S., Hólm, E., Hoskins, B. J., Isaksen, L., Janssen, P. A. E. M., Jenne, R., Mcnally, A. P., Mahfouf, J.-F., Morcrette, J.-J., Rayner, N. A., Saunders, R. W., Simon, P., Sterl, A., Trenberth, K. E., Untch, A., Vasiljevic, D., Viterbo, P., and Woollen, J.: The ERA-40 re-analysis, Q. J. Roy. Meteor. Soc., 131, 2961–3012, 2005.

van Bennekom A. J., Buma, A., and Nolting, R.: Dissolved aluminium in the Weddell-Scotia Confluence and effect of Al on the dissolution kinetics of biogenic silica, Mar. Chem., 35, 423–434, 1991.

van Beusekom J. E. E. and Weber, A.: Decreasing diatom abundance in the North Sea: the possible significance of aluminium, Olsen. Int. S., 121–127, 1992.

van Cappellen P., Dixit, S., and van Beusekom, J.: Biogenic silica dissolution in the oceans: Reconciling experimental and field-based dissolution rates, Global Biogeochem. Cy., 16, 1075, doi:10.1029/2001GB001431, 2002.

van Hulten, M. M. P., Sterl, A., Dutay, J.-C., Tagliabue, A., Gehlen, M., de Baar, H. J. W., and Middag, R.: Aluminium in an ocean general circulation model compared with the West Atlantic Geotraces cruises, J. Mar. Syst., 126, 3–23, doi:10.1016/j.jmarsys.2012.05.005, 2013.

Vink, S. and Measures, C.: The role of dust deposition in determining surface water distributions of Al and Fe in the South West Atlantic, Deep-Sea Res. Pt. II, 48, 2787–2809, 2001.

Vrieling, E., Poort, L., Beelen, T., and Gieskes, W.: Growth and silica content of the diatoms Thalassiosira weissflogii and Navicula salinarum at different salinities and enrichments with aluminium, Eur. J. Phycol., 34, 307–316, 1999.

Wedepohl, K.: The composition of the continental crust, Geochim. Cosmochim. Ac., 59, 1217–1232, 1995.